FEATURE ARTICLE

Ultrafast Electron Dynamics and Optical Nonlinearities in Metal Nanoparticles

Christophe Voisin,[†] Natalia Del Fatti,[†,‡] Dimitris Christofilos,[†] and Fabrice Vallée*[,†,‡]

Laboratoire d'Optique Quantique du CNRS, Ecole Polytechnique, 91128 Palaiseau, France, and CPMOH, CNRS-Université Bordeaux I, 351 cours de la Libération, 33405 Talence, France

Received: October 19, 2000; In Final Form: January 9, 2001

The femtosecond optical response of noble metal nanoparticles and its connection to the ultrafast electron dynamics are discussed in light of the results of high-sensitivity femtosecond pump−probe experiments. The physical origins of the nonlinear responses in the vicinity of the surface plasmon resonance and interband transition threshold are analyzed using extension of the theoretical models used in the bulk materials. These responses contain information on the electron interaction processes (electron−electron and electron−phonon scattering) that can thus be directly investigated in the time domain. Their size and environment dependences are discussed, and the results are compared to the ones in the bulk materials. Time-resolved techniques also permit direct study of the vibrational modes of metal nanoparticles and, in particular, the determination of their damping, which is a sensitive probe of the nature of the surrounding matrix and of the interface quality.

I. Introduction

Most of the physical properties of homogeneous bulk materials are associated with characteristic lengths, such as nuclear and electronic mode wavelengths (Debye and Fermi wavelengths), delocalization and screening lengths or mean free paths, which reflect intrinsic constraints on the charge or ion motion imposed by their structure or composition. These lengths also roughly define the scale over which the boundaries of a finite size media play a minor role in a specific process, which is then identical to the one in the bulk. Artificial nanomaterials with characteristic sizes well below these lengths can now be grown and, as expected, exhibit size-dependent properties. This offers the unique possibility to purposely alter the properties of reduced dimensionality systems, and even control them to meet technological requirements or perform certain functions, making them a very important class of materials for technological applications.[1−4]

An important aspect here is the increasing coupling of a confined object with its environment as its size decreases, and, in particular, the increasing role of energy or charge exchanges at its interface. Understanding and modeling of these size and environment effects are also very interesting from the fundamental point of view, especially in the case of nanoparticles or clusters that constitute intermediate systems between molecules and bulk materials and offer the possiblity to continuously follow the material property evolution with confinement. Of particular interest are the impacts of the confinement and environment on the electron interactions and the related energy redistribution processes. With the advance of the femtosecond lasers, these can now be directly and selectively investigated using femtosecond optical techniques.

Metal and semiconductor nanoparticles have been extensively studied, in particular in the optical domain. Here, the most conspicuous consequence of the confinement is the appearance of morphological resonances related either to quantum or dielectric confinement effects.[4−12] Conversely to semiconductor systems, quantum (i.e., electron) confinement plays a small role in the large metal clusters (diameter larger than 2 nm, i.e., formed by more than 250 atoms) considered here and can be introduced as a correction. This is a consequence of the large density of electronic states around the Fermi energy in a metal that permits us to describe the electron response by defining a quasi-continuum of states and thus to use a bulklike description. In the case of metal nanocrystals, the morphological resonance is the surface plasmon resonance (SPR) which is a direct consequence of the dielectric confinement (i.e., of the local field effect) and strongly influences their linear and nonlinear optical responses.[8−12] The SPR spectral characteristics (frequency, shape, width) are influenced by the impact of the boundaries on the electron properties and its dynamics is thus largely connected to the electron one in the confined material.

Femtosecond techniques have been extensively used to investigate the different elementary scattering mechanisms in bulk metal,[13−20] and, recently metal nanoparticles.[21−32] These are based on selective electron excitation on a time scale shorter than that of electron−electron and electron−lattice energy redistributions (i.e., the lattice and matrix are not directly heated). The injected energy is subsequently redistributed among the electrons by electron−electron (e−e) scattering eventually leading to the establishment of an electron temperature, and transferred to the lattice by electron−phonon (e−ph) interactions, leading to thermalization of the metal electron gas and lattice (Figure 1). These two processes usually take place on similar time scales (for instance, about 0.5 and 1 ps, respectively, in gold[15]) and mutually influence each other on a subpicosecond time scale.[16,19,20] They can be selectively followed by monitoring the transient optical properties of the material and information has been obtained on electron−phonon,[15−20] and electron−

[†] Ecole Polytechnique.
[‡] CNRS-Université Bordeaux I.

10.1021/jp0038153 CCC: $20.00
Published on Web 03/02/2001

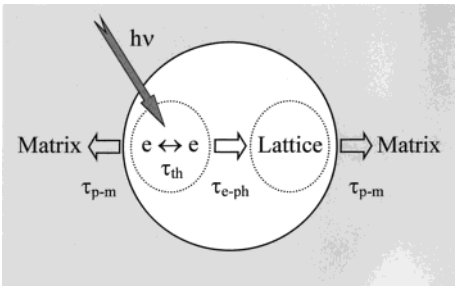

Figure 1. Sketch of the energy relaxation processes after selective excitation of nonequilibrium electrons by a femtosecond pulse ($h\nu$) in a metal nanoparticle. τ_{th}, τ_{e-ph}, and τ_{p-m} are the characteristic times for internal thermalization of the electron gas, electron−lattice thermalization, and particle−matrix energy exchanges, respectively.

electron scattering,[15,16,20] and also on electron spin relaxation[33−36] and electronic transport[37,38] in bulk metals.

The aim of this paper is not to give an exhaustive review of this rapidly growing field but to discuss the ultrafast electron dynamics and its connection with the ultrafast SPR optical nonlinearities in relatively large metal nanoparticles (more than few hundred atoms). This will be done on the basis of the results of femtosecond investigations performed in the low perturbation regime in noble metals (Ag and Au). In this regime the nanoparticle optical response can be simply modeled and directly compared for different sizes. Furthermore, as these not too small metal objects can be conveniently described using a small solid approach, rather than a molecular one for a few atom clusters, their responses can also be directly compared to the bulk material ones, permitting us to trace the first impacts of the dielectric and quantum confinements on the electron interaction processes and ultrafast nonlinear optical response.

After electron−lattice thermalization, the time-domain response of metallic systems is dominated by their coherent acoustic vibration and energy exchanges with their environment (matrix or substrate, Figure 1). The former effect, associated with acoustic mode quantization, takes place on a few to few tens of picoseconds[39−43] and will be discussed in the case of nanoparticles in section VI. The latter effect, that is the last step to full thermalization of a composite material is an important parameter for many applications but will not be discussed here, as it usually takes place on a much longer time scale (few tens to few hundred picoseconds depending on the particle size, matrix heat conductivity and interface quality).[8,44−46]

II. Optical Properties of Metal Nanoparticles

A. Linear Properties. The optical properties of metallic systems are determined by the conduction and bound electron responses. In bulk noble metals, the conduction electrons follow a quasi-free electron behavior and their contribution to the dielectric constant at the frequency ω is well described by a Drude formula[47,48]

$$\epsilon^{f}(\omega) = 1 - \frac{{\omega_p}^2}{\omega[\omega + i/\tau_o(\omega)]} \tag{1}$$

where ω_p is the plasma frequency (${\omega_p}^2 = n_e e^2/\epsilon_0 m$, n_e and m being the conduction electron density and effective mass, respectively). $\tau_o(\omega)$ is the electron optical relaxation time, which is determined by electron−phonon and electron−electron scattering (neglecting electron−defect scattering) with simultaneous exchange of the energy $\hbar\omega$ of a photon.[49−51] The probability of photon absorption is proportional to $1/\tau_o$ since it has to be assisted by a third quasi-particle (phonon or electron) to satisfy energy and momentum conservations. Assuming the contributions to τ_o uncorrelated, we can write[49−52]

$$\frac{1}{\tau_o(\omega)} = \frac{1}{\tau_{e-ph}(\omega)} + \frac{1}{\tau_{e-e}(\omega)} \tag{2}$$

In thermal equilibrium at room temperature, τ_{e-ph} is much smaller than τ_{e-e} and yields the main contribution to $1/\tau_o$[49] (only umklapp processes contribute to τ_{e-e}[50]). The presence of the bound electrons leads to an additional contribution to ϵ so that the complete dielectric constant is[53]

$$\epsilon(\omega) = \epsilon^{f}(\omega) + \delta\epsilon^{b}(\omega) \tag{3}$$

In noble metals, the main contribution to the bound electron term, $\delta\epsilon^b$, is associated with the interband transitions from the fully occupied d-bands below the Fermi energy to the half filled s−p conduction band (Figure 2a, inset).[47]

The metal properties related to the quasi-free electrons are modified in a nanocrystal due to their interaction with the interface and the concomitant breakdown of the system periodicity. The impact of confinement on the optical response can be accounted for by different approaches, classical or quantum mechanical,[5−9,54,55] all leading to the same result that the intraband contribution to the dielectric constant of a metal nanocrystal preserves its Drude form (1) with the scattering time now being

$$\frac{1}{\tau(\omega)} = \frac{1}{\tau'_o(\omega)} + \frac{V_F}{R} g_S(\omega) \tag{4}$$

The first term, τ'_o, reflects bulklike electron scattering in the particle (eq 2), with the interaction rates possibly altered by confinement (section V). The second term is proportional to the Fermi velocity V_F divided by the radius R of the assumed spherical nanoparticle, with a frequency and electron distribution-dependent proportionality factor g_S of the order of 1[9,54] (see section II.D.2). It is a direct consequence of the limitation of the electron motion. Classically, it can be interpreted as being due to electron scattering off the surface whose probability becomes comparable to the other scattering processes in sufficiently small nanoparticles (using $\tau'_o \approx 10$ fs in noble metals[49] and $g_S \approx 1$,[9] the two contributions are identical for $R \approx 15$ nm). Optical absorption is thus induced due to breaking of wave vector conservation by the surface. In a more correct quantum mechanical description, this term is a consequence of the fact that in a particle the wave functions of electrons in a well have to be used instead of the Bloch ones in the bulk. The wave vector is no more a good quantum number and photon absorption is then possible without any collision.[5,10,54,55] It corresponds to transitions between confined electronic states enhanced by the local field effect. This term is thus a manifestation of quantum confinement in the metal nanoparticle optical response.

For not too small particles ($R \geq 1.5$ nm), modification of the interband transition spectrum can be neglected.[56,57] The crystallite dielectric constant takes a similar form as the bulk one (eq 3) using the bulk $\delta\epsilon^b$ and replacing τ_o by τ in (1).[57,58] This expression of ϵ will be used in the following to discuss the metal nanoparticle optical properties.

In most experiments one is dealing with an ensemble of nanoparticles dispersed in a liquid or solid matrix or deposited on a substrate. For a low volume fraction $p \ll 1$ of small spheres ($R \ll \lambda$, where λ is the optical wavelength, so that the quasi-static approximation can be used), one can introduce an effective

dielectric constant for the composite material which, in the effective medium approach, is given by[5−9,11,59]

$$\tilde{\epsilon}(\omega) = \epsilon_d + 3p\epsilon_d \frac{\epsilon(\omega) - \epsilon_d}{\epsilon(\omega) + 2\epsilon_d} \quad (5)$$

where ϵ_d is the matrix dielectric constant and will be assumed frequency-independent and real. The composite material absorption coefficient can then be written[9−11]

$$\tilde{\alpha}(\omega) = \frac{9p\epsilon_d^{3/2}}{c} \frac{\omega\epsilon_2(\omega)}{[\epsilon_1(\omega) + 2\epsilon_d]^2 + \epsilon_2^2(\omega)} \quad (6)$$

where $\epsilon(\omega) = \epsilon_1(\omega) + i\epsilon_2(\omega)$. This expression corresponds to keeping only the dipolar terms in Mie's theory[60,61] and is thus valid only for small particles ($2R \leq \lambda/10$[54]). The scattering term (or radiative damping effect) has been omitted, as it plays a negligible role for the investigated sizes.[5] As compared to the bulk metal, the absorption is resonantly enhanced close to the frequency, Ω_R, minimizing the denominator, which is the condition for the surface plasmon resonance (SPR). This is concomitant with enhancement of the electric field inside the particle as compared to the applied field and can be described in terms of a local field effect.[8−11] It corresponds to coherent superposition of the electromagnetic and material excitations (i.e., resonant fluctuations of the electron density) similar to polariton excitation in bulk material.[62]

The absorption spectrum of noble metal nanoparticles is well reproduced using (6) with the measured bulk dielectric constant[48,63] and including the surface correction (eq 4, where g_S is used as a parameter, Figures 2 and 3). For a small or weakly dispersed ϵ_2 around Ω_R, the SPR frequency is determined by the condition[5−11]

$$\epsilon_1(\Omega_R) + 2\epsilon_d = 0 \quad (7)$$

Separating ϵ into its interband and intraband terms (3), one obtains

$$\Omega_R = \frac{\omega_p}{\sqrt{\epsilon_1^b(\Omega_R) + 2\epsilon_d}} \quad (8)$$

where $\epsilon_1^b = 1 + \delta\epsilon_1^b$. Because of the large frequency threshold for the interband transitions in silver ($\hbar\Omega_{ib} \approx 4$ eV), the SPR lies in an isolated region of the spectrum and shows up as a well-defined resonance (Figure 2). This is in contrast to other noble metals where the SPR partly overlaps the interband transitions, as shown for gold colloids in Figure 3.

The general expression of the absorption (eq 6) can be greatly simplified if ϵ_1^b is weakly dispersed around Ω_R (i.e., $(\partial\epsilon_1^b/\partial\omega/_{\Omega_R} \ll 2\omega_p^2/\Omega_R^3$). The SPR then takes a quasi-Lorentzian shape:

$$\tilde{\alpha}(\omega) = \frac{A\omega^2\Omega_R^4\Gamma}{(\omega^2 - \Omega_R^2)^2 + (\Omega_R^2\Gamma/\omega)^2} \quad (9)$$

where $A = 9p\epsilon_d^{3/2}/c\omega_p^2$. This approximation can be performed for silver (but not for other noble metals) and yields a good reproduction of the experimental absorption spectrum in the vicinity of Ω_R (Figure 2).

In this description, the SPR width, Γ, is proportional to $\epsilon_2(\Omega_R)$ and is the sum of an interband term proportional to $\epsilon_2^b(\Omega_R)$ and of an intraband one γ:

$$\Gamma = \frac{\Omega_R^3}{\omega_p^2}\epsilon_2^b(\Omega_R) + \gamma(\Omega_R) \quad (10)$$

where $\gamma(\omega) = 1/\tau(\omega)$. Electron−surface scattering (with $\gamma_S = g_S V_F/R$, eq 4) yields an important contribution to Γ and is responsible for its increase with R for small nanoparticles.[5−9] In contrast, for the investigated sizes ($1.5 \leq R \leq 15$ nm), the SPR frequency is almost independent of R.[64,65] Size distribution in a sample mainly reflects in fluctuations of Γ and thus leads to a larger contribution of the small particles in the wings of the SPR line than at the center, necessitating the use of samples

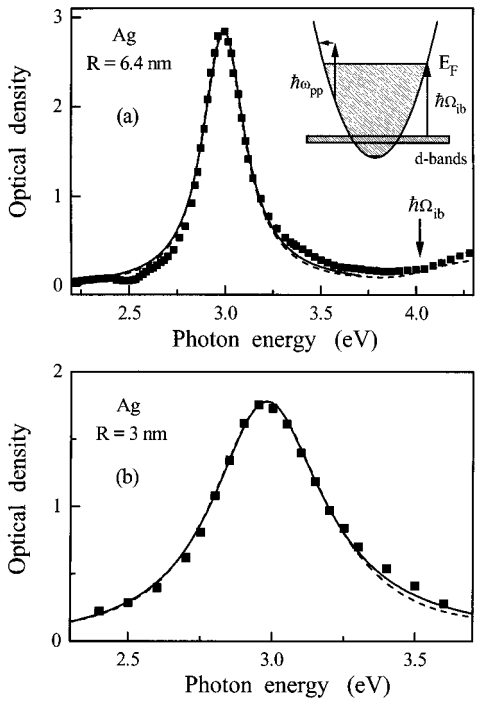

Figure 2. Measured absorption spectrum of $R = 6.4$ nm (a) and 3 nm (b) silver nanoparticles embedded in a $50BaO-50P_2O_5$ glass matrix (squares). The absorption rise for high energy ($\hbar\omega > \hbar\Omega_{ib} \approx 4$ eV) is due to the onset of the interband transitions. The dashed lines are calculated using (6) with the measured bulk silver dielectric constant and including the surface term (eq 4, where g_S is used as a parameter). The full lines are fits of the absorption around $\hbar\Omega_R$ assuming a quasi-Lorentzian SPR line shape (9). The inset shows a schematic electron band structure of noble metals where $\hbar\Omega_{ib}$ is the interband transition threshold between the top of the d-bands to the Fermi surface (E_F). The left arrow indicates intraband electron excitation by $\hbar\omega_{pp}$ photons.

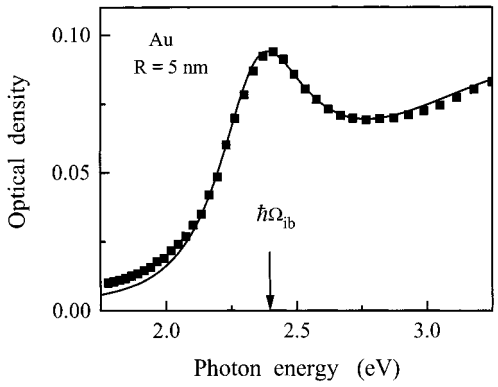

Figure 3. Measured (squares) and calculated (using (6) and (4), full line) absorption spectrum for $R = 5$ nm gold nanoparticles in solution. The arrow indicates the interband absorption threshold $\hbar\Omega_{ib}$.

with a well-controlled size dispersion. Environment effects are very important here and it has been shown that γ_S, and thus Γ, strongly depends on the nature of the surrounding media (i.e., vacuum, solvent, glass).[9,57] This dependence is not predicted by the quantum mechanical models that include only internal particle effects and has been attributed to chemical damping.[57] Environment fluctuations can also lead to local changes of ϵ_d and thus of Ω_R (eq 8), inducing an inhomogeneous broadening of the SPR line, as observed for porous matrixes.[66,67]

In the equilibrium situation, the first term in (10) is negligible in silver since the SPR lies well below Ω_{ib} (Figure 2). This separation between the interband and SPR effects greatly simplifies interpretation of the ultrafast response of silver nanoparticles, making them model systems for analyzing the SPR and electron dynamics.

B. Femtosecond Electron Excitation. In our femtosecond experiments, we selectively perturb the electron distribution by intraband absorption of a pump pulse of frequency ω_{pp} much smaller than Ω_{ib} (Figure 2a, inset). Coherent coupling of the electromagnetic field and collective electron motion initially takes place. The induced polarization decays with the electron scattering time τ (i.e., in a sub 10 fs time scale in nanoparticles), in agreement with time-resolved nonlinear investigations[68−70] and hole burning measurements.[71] This decay takes place with single electron excitation,[5] and we have shown that, for excitation either in or out of resonance with the SPR, this coherent stage does not affect our measurements (with 20−30 fs pulses) and only single quasi-free electron excitation is observed.[72] In both metal films and nanoparticles, only incoherent effects have thus to be taken into account and the pump−pulse absorption can always be described in terms of free-electron absorption (Figure 2a, inset).

Femtosecond excitation thus leads to the creation of a strongly athermal electron distribution,[15,72] with electrons with an energy E between $E_F - \hbar\omega_{pp}$ and E_F being excited above the Fermi energy with a final energy between E_F and $E_F + \hbar\omega_{pp}$ (Figure 4). Electron−electron scattering redistributes the energy in the electron gas, eventually leading to a hot Fermi distribution with temperature T_e (the characteristic thermalization times are ∼500 and 350 fs in bulk Au and Ag, respectively[15,20,73]). During and after internal thermalization, energy is transferred to the lattice by electron−phonon interaction, with a characteristic time of about 1 ps in bulk noble metals. On a short time scale (≤1 ps), the internal and external energy redistribution processes have to be treated on the same footing. This can be done using the Fermi liquid theory and by describing the conduction electron system by a one-particle distribution function f whose time evolution is given by the Boltzmann equation:

$$\frac{df(E)}{dt} = \left.\frac{df(E)}{dt}\right|_{e-e} + \left.\frac{df(E)}{dt}\right|_{e-ph} + H(E,t) \qquad (11)$$

$H(E,t)$ stands for the perturbation by the pump pulse:

$$H(E,t) = BI_p(t)\{\sqrt{E-\hbar\omega_{pp}}f(E-\hbar\omega_{pp})[1-f(E)] - \sqrt{E+\hbar\omega_{pp}}f(E)[1-f(E+\hbar\omega_{pp})]\} \qquad (12)$$

where $I_p(t)$ is the pump pulse intensity and B is a constant. For instantaneous excitation, the step like f change shown in Figure 4 is obtained.

Although the electrons are initially not thermalized, it is convenient to characterize the excitation amplitude by defining a maximum equivalent T_e rise, ΔT_e^{me}, as the temperature rise of a thermalized electron gas for the same energy increase. Taking into account the temperature dependence of the electron heat capacity $C_e(T_e) = aT_e$, ΔT_e^{me} is given by

$$\Delta T_e^{me} = [T_0^2 + 2N_{pp}\hbar\omega_{pp}/a]^{1/2} - T_0 \qquad (13)$$

where T_0 is the initial temperature and N_{pp} is the number of absorbed pump photons per unit volume. C_e being much smaller than the lattice heat capacity C_L, the final temperature rise $T_L - T_0$ of the fully thermalized electron−lattice system is always much smaller than ΔT_e^{me} ($T_L - T_0$ is of the order of $C_e\Delta T_e^{me}/C_L \sim \Delta T_e^{me}/100$).

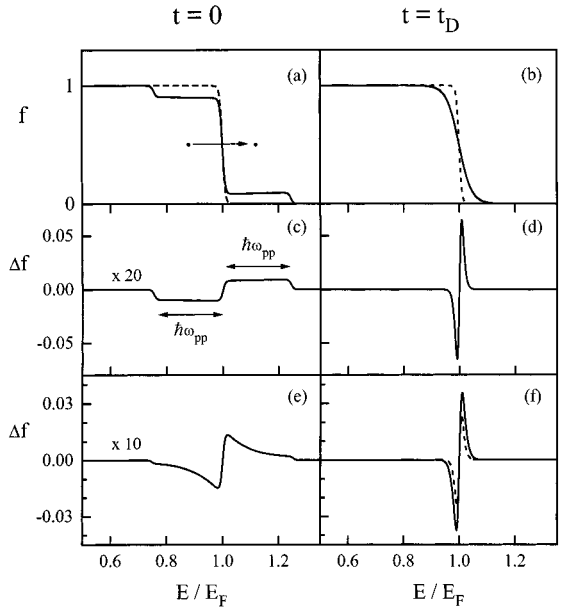

Figure 4. (a) Equilibrium (f_0, dashed line) and initial athermal (f, full line) electron occupation number assuming instantaneous intraband excitation by a pump pulse of frequency ω_{pp}, with $\hbar\omega_{pp} = 0.24E_F$. (b) Same as (a) after establishment of an electron temperature (after a delay t_D). (c) and (d) show the corresponding distribution change $\Delta f = f - f_0$ around E_F for the athermal and thermal situations, respectively (the same total electron energy is assumed). (e) Δf computed at $t_D = 0$ fs in Ag using the model of section II.B for $\Delta T_e^{me} = 100$ K and a $\hbar\omega_{pp} = 1.3$ eV pump pulse with duration $t_p = 25$ fs. (f) Same as (e) for $t_D = 400$ fs and 1 ps (full and dashed line, respectively).

C. Femtosecond Electron Dynamics. The time-dependent electron distribution change, Δf, can be computed using (11) and taking into account the finite pump pulse duration t_p (Figure 4, where the bulk silver e−e, $(df/dt)_{e-e}$, and e−ph, $(df/dt)_{e-ph}$, scattering rates were used[20]). As expected, Δf initially extends over a very broad energy range, with a shape modified by electron relaxation during the pulse duration (Figure 4e, for $t_D = 0$, defined as the pump pulse maximum). This is a consequence of the very fast relaxation of electrons with energy E far from E_F, the E dependence of the e−e scattering rate being of the form $\gamma_{rel}(E) \propto (E - E_F)^2$ with $\gamma_{rel}(E_F + 1\text{ eV}) \approx 20$ fs[20,73−78] (note that the "holes" with an energy $E_F - E_h$ exhibit a similar dynamics as the electrons with energy $E_F + E_h$[20]). Δf subsequently strongly narrows as the electron gas internally thermalizes, the perturbed zone being eventually limited to a region of the order of k_BT_e around E_F.

An important point here is that the electron relaxation dynamics is independent of the injected energy for $\Delta T_e^{me} \leq$ 200−300 K (weak perturbation regime). For larger energy injection, it depends on the excitation amplitude as a consequence of the dependence of the electron scattering rates on the electron distribution.[20] In this nonlinear regime, acceleration of the internal thermalization of the electron gas and slowing

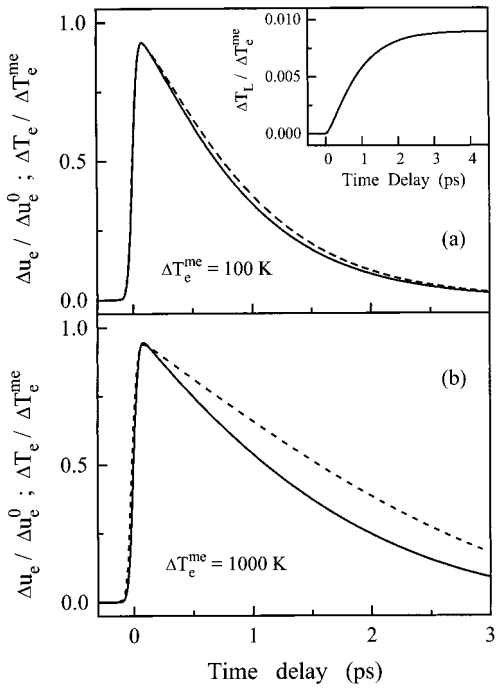

Figure 5. Normalized time dependence of the electron excess energy, Δu_e (full line), computed using the model of section II.B for electron excitation with a 25 fs pump pulse and $\Delta T_e^{me} = 100$ K (a) and 1000 K (b). Δu_e^0 is the total energy absorbed by the electrons. The dashed lines show the correlated electron temperature rise $\Delta T_e(t_D) = [T_0^2 + 2\Delta u_e(t_D/a]^{1/2} - T_0$ (note that T_e is correctly defined only for $t_D \geq 0.5$ ps). The inset shows the corresponding time dependence of the normalized lattice temperature (for $\Delta T_e^{me} = 100$ K).

down of its cooling have been demonstrated in films[17,20,79] and nanoparticles.[29−31,80−82] The latter point is illustrated in Figure 5 showing the time evolution of the excess energy, $\Delta u_e(t_D)$, of the electron gas computed for $\Delta T_e^{me} = 100$ K and 1000 K ($\Delta u_e(t_D)$ is defined as the difference between the electron gas energy at time t_D and the one before perturbation).

This behavior is a consequence of the T_e dependence of the electronic heat capacity C_e[29−31,80−82] and, after internal thermalization, can be discussed using the two-temperature model.[83] The electron gas is then entirely described by its temperature and its cooling dynamics can be simply modeled using the rate equation system:

$$C_e(T_e)(\partial T_e/\partial t) = -G(T_e - T_L)$$
$$C_L(\partial T_L/\partial t) = G(T_e - T_L) \qquad (14)$$

where G is the effective electron−phonon coupling constant. It only describes electron−lattice energy exchanges and is a consequence of the Boltzmann equation (11).[83] It is fully equivalent to the above more general model when T_e can be defined (i.e., for $t_D \geq 0.5-1$ ps). For a weak perturbation, $C_e(T_e)$ can be identified with $C_e(T_0)$ leading to exponential decays of ΔT_e and Δu_e with the same time constant $\tau_{e-ph}^0 \approx C_e(T_0)/G$ (eq 14 and Figure 5). This is in agreement with the results in noble metal films and permits direct measurement of τ_{e-ph}^0 and thus of G.[15,16,19,20]

In contrast, for strong excitation, the T_e dependence of C_e has to be taken into account. It leads to a nonexponential T_e decay with a large perturbation-dependent slowing down of its short time delay dynamics (Figure 5). Furthermore, the relation between ΔT_e and Δu_e is nonlinear and they thus exhibit different time dependences (Figure 5). This is eventually followed by

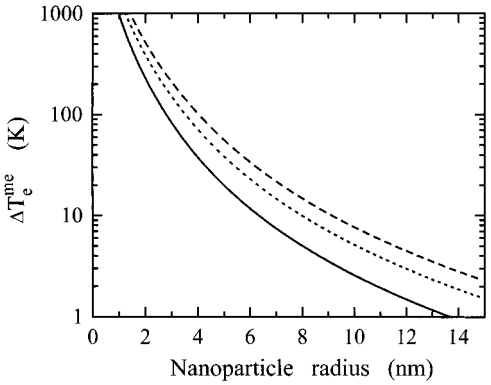

Figure 6. Maximum equivalent electron temperature rise ΔT_e^{me} induced by absorption of 1 (full line), 2 (dotted line), and 3 (dashed line) near-infrared photons ($\hbar\omega_{pp} = 1.3$ eV) in a spherical silver particle as a function of its radius (using (13) with $a = 65$ J/(m^3 K^{-2})).

an exponential decay of both ΔT_e and Δu_e with the same time constant τ_{e-ph}^0 as T_e approaches T_L and the weak perturbation approximation can again be used.[20] In this nonlinear regime, quantitative extraction of the intrinsic electron relaxation time constants (τ_{e-ph}^0 or G, in particular) is difficult, since it requires a precise knowledge of the injected energy, i.e., ΔT_e^{me}, and of the origin of the measured signal (i.e., if it is related to ΔT_e or Δu_e).

A simple consequence of the confinement of the electron motion is that the injected energy is initially localized in the nanoparticles since excitation is much faster than energy transfer to the surrounding matrix. The minimum energy injection in a nanoparticle corresponds to absorption of one photon. There is thus a minimum ΔT_e^{me} that can be induced in each excited particle (i.e., the ones contributing to the measured signal), that is set by the pump photon energy and R (Figure 6). This can be fairly large and already corresponds to the strong excitation regime for small sizes. Conversely to bulk materials, independence of the transient response shape on the pump fluence is not sufficient in nanoparticles to characterize the weak perturbation regime (since below a certain fluence only the number of excited particles is reduced but not their excitation level), but one has to check that it is also independent of $\hbar\omega_{pp}$.

The above electron dynamics modeling has been developed for bulk materials. To a large extent, it is expected to be also applicable to not too small objects where the main band structure features of the bulk material are retained (at least for $R \geq 1.5$ nm). As a first approximation, it can be used for interpreting the ultrafast response in metal particles.[28,84] One has, however, to keep in mind that this approach overlooks specific features of the electron dynamics in confined systems, and, in particular, the size dependence of the efficiency of the electron scattering processes (see section V).

D. Nonlinear Optical Response. In the time-resolved experiments described here, the time-dependent changes of the sample optical properties (transmission, T, and/or reflectivity, R) are monitored using a delayed probe pulse of frequency ω_{pr}. They reflect alteration of the dielectric constant of the material, i.e., its nonlinear optical response. It is usually sufficiently weak to use a perturbational approach,[14] and in a composite material, the transmission change $\Delta T/T$ is connected to $\tilde{\epsilon}$ by

$$\frac{\Delta T(t_D)}{T} = \frac{\partial \ln T}{\partial \tilde{\epsilon}_1}\Delta\tilde{\epsilon}_1(t_D) + \frac{\partial \ln T}{\partial \tilde{\epsilon}_2}\Delta\tilde{\epsilon}_2(t_D) \qquad (15)$$

with a similar expression for $\Delta R/R$. $\Delta T(t_D)$ is defined as the

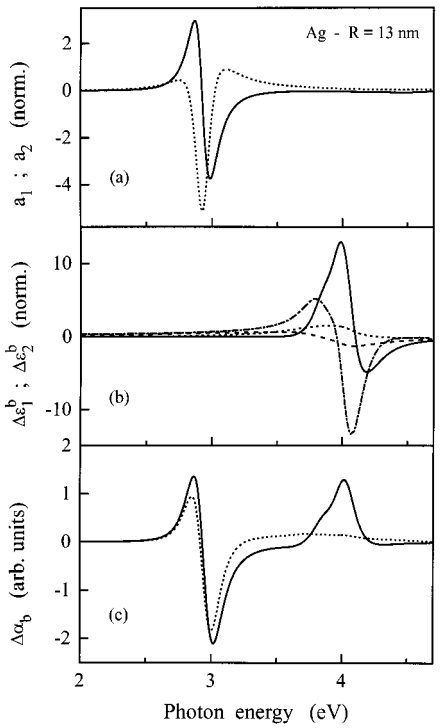

Figure 7. (a) Dispersion of the coefficients a_1 (full line) and a_2 (dashed line) linking $\Delta\tilde{\alpha}$ to $\Delta\epsilon_1$ and $\Delta\epsilon_2$ (16) for $R = 13$ nm silver nanoparticles. (b) Interband contribution to $\Delta\epsilon_1$ and $\Delta\epsilon_2$ for $t_D = 0$ fs (dashed and dotted lines) and $t_D = 400$ fs (dash−dotted and full lines). The corresponding transient electron distribution changes are shown in Figure 4e,f. The Rosei band structure model has been used to connect $\Delta\epsilon_2^b$ to Δf (section II.D.1. (c) Corresponding absorption change due to only the interband contribution $\Delta\alpha_b = -(\Delta T/T)_b/L$ (16).

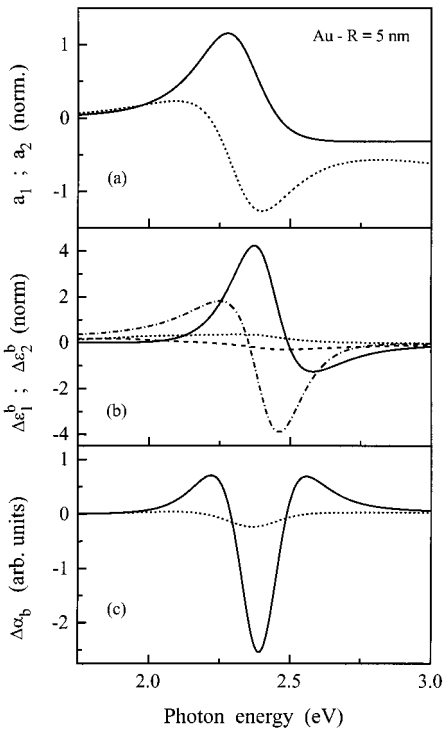

Figure 8. Same as Figure 7 for $R = 5$ nm gold nanoparticles in solution (see Figure 3).

difference between the sample transmission at time t_D minus the one without perturbation.

In dilute composite materials one can show that the first term is negligible (this is actually a consequence of their low reflectivity and small nanoparticle contribution to $\tilde{\epsilon}_1 \approx \epsilon_d$, eq 5). $\Delta T/T$ is thus only determined by $\Delta\tilde{\epsilon}_2$, or, equivalently, by the sample absorption change:

$$\Delta T/T = -\Delta\tilde{\alpha}L = -a_1\Delta\epsilon_1 - a_2\Delta\epsilon_2 \qquad (16)$$

where L is the sample thickness and ϵ_d has been assumed constant. It is a linear combination of the changes of the real and imaginary parts, $\Delta\epsilon_1$ and $\Delta\epsilon_2$, of the metal nanoparticle dielectric function. The coefficients $a_1 = (\partial\tilde{\alpha}/\partial\epsilon_1)L$ and $a_2 = (\partial\tilde{\alpha}/\partial\epsilon_2)L$ (Figures 7 and 8), are entirely determined using eq 6 and the ϵ_1 and ϵ_2 values used for fitting the linear absorption spectrum (Figure 2 and 3).

To model the experimental results, one has to connect $\Delta\epsilon(t_D)$ to the computed distribution change $\Delta f(t_D)$ (section II.B) and to the lattice heating ΔT_L. Both the interband and intraband contributions to ϵ depend on f and T_L and, for a weak damping ($\gamma_f \ll \omega$), one can write

$$\Delta\epsilon_1(\omega) \approx \Delta\epsilon_1^b(\omega) - (2\omega_p/\omega^2)\Delta\omega_p$$
$$\Delta\epsilon_2(\omega) \approx \Delta\epsilon_2^b(\omega) + (\omega_p{}^2/\omega^3)\Delta\gamma(\omega) \qquad (17)$$

Electron distribution change effects dominate the short time scale response[19,20] (for interband excitation, the ω_p increase due to excitation of d-electrons into the conduction band also gives a contribution that decays in a few tens of femtoseconds with electron recombination with d-holes.[77,85] It will be not considered here). On a longer time scale, the system reaches thermal equilibrium with a small temperature rise ($\Delta T_e = \Delta T_L \ll \Delta T_e^{me}$) considerably reducing the amplitude of the electronic effects. Lattice heating and the concomitant lattice expansion then also play important roles. The interband, $(\Delta T/T)_b$ (or $\Delta\alpha_b$), and intraband, $(\Delta T/T)_f$ (or $\Delta\alpha_f$), contributions to $\Delta T/T$ (or $\Delta\tilde{\alpha}$) will be discussed in the next sections.

1. Nonlinear Optical Response: Interband Contribution. In bulk noble metal, interband absorption is dominated by transitions from the full d-bands to empty states in the conduction band (Figure 2a, inset).[47] Around the interband transition threshold $\hbar\Omega_{ib}$, it is determined by the occupation of the electronic states close to E_F. Electron excitation leads to electron distribution smearing with reduction (increase) of the occupation number of the states below (above) E_F (Figure 2). Consequently, absorption is induced (reduced) for transitions involving final states below (above) E_F.[14,15] Around $\hbar\Omega_{ib}$, absorption has been shown to be dominated by transitions from the upper d-band to the Fermi surface in the vicinity of the L point of the Brillouin zone. Rosei and co-workers have modeled the bulk band structure around this point in silver and gold for interpreting CW thermomodulation measurements.[86−88] This model permits us to calculate $\Delta\epsilon_2^b$ from Δf, $\Delta\epsilon_1^b$ being then obtained using the Kramers−Kronig relationship. The same approach has been used to model the femtosecond response of noble metals using a time-dependent Δf.[15,16,20,28,31] The computed spectra of $\Delta\epsilon_1^b$ and $\Delta\epsilon_2^b$ for $t_D = 0$ and 400 fs are shown in Figures 7 and 8 for bulk silver and gold.[15,20]

For not too small particles the same model can be used to compute $\Delta\epsilon^b$ and the interband contribution $(\Delta T/T)_b$ to $\Delta T/T$ using (16). In silver, the computed $(\Delta T/T)_b$ exhibits two distinct spectral features around Ω_{ib} and Ω_R with very different time behaviors (Figure 7). The former is similar to that observed in the bulk material and its time behavior is related to the internal electron thermalization dynamics (see section V.A). It corresponds to resonant probing of the interband transitions and its strong dispersion reflects that of $\Delta\epsilon^b$. In contrast, the structure

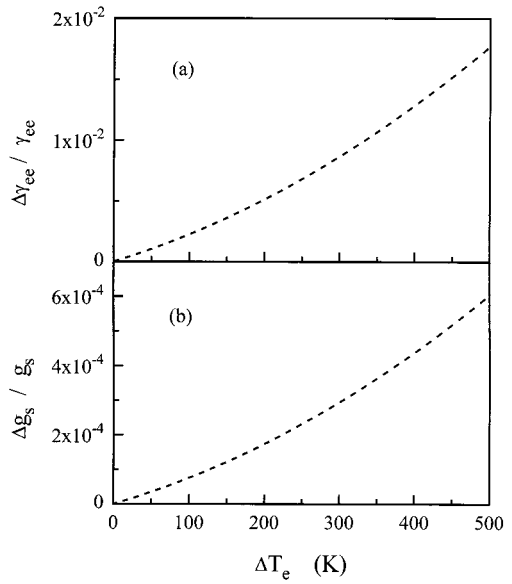

Figure 9. Relative change of the electron−electron (a) and electron−surface (b) scattering rates, computed in Ag using (20) and (19), as a function of the electron temperature rise $\Delta T_e = T_e - T_0$ where T_0 is the room temperature.

around Ω_R is a consequence of the enhancement of the nonlinear optical response around the SPR due to the dielectric confinement[8] and is specific to confined systems. It is actually due to the large amplitude and dispersion of a_1 and a_2 around Ω_R, where $\Delta\epsilon^b$ is small and almost undispersed since it corresponds to probing off resonance with the interband transitions. In the case of gold, the SPR is close to Ω_{ib} and these two features overlap (Figure 8). A similar shape is expected for copper, which exhibits the same degeneracy between the interband transitions and SPR.[4,7,8]

2. Nonlinear Optical Response: Intraband Contribution. The probabilities of all the electron scattering processes depend on the electron distribution and lattice temperature T_L,[49−52] and, most generally, $\Delta\gamma$ can be written

$$\Delta\gamma = \Delta\gamma_{e-ph}(T_e,T_L) + \Delta\gamma_{e-e}(T_e) + \Delta\gamma_S(T_e) \qquad (18)$$

where $\gamma_S = g_S V_F/R$. The Fermi velocity being almost unchanged (since $\Delta T_e^{me} \ll T_F$[47]), the f dependence of γ_S reflects that of g_S (eq 4). This has been calculated for a zero electron temperature using different approximations.[5−9,54,55] Extending the Kawabata and Kubo approach,[5] we have shown that eq 4 can be generalized to finite temperatures using

$$g_S(\omega) = \frac{1}{\hbar\omega}\int_0^\infty \frac{E^{3/2}(E+\hbar\omega)^{1/2}}{E_F^{\,2}} f(E)[1 - f(E+\hbar\omega)]\, dE \qquad (19)$$

This dependence of γ_S on the electron distribution is similar to the ones of the other scattering processes[50,51,53] and is a consequence of the Pauli exclusion principle. These f dependences are, however, much weaker than for the dc electron scattering rate $\gamma(\omega = 0)$,[52] since the involved initial and final electronic states are separated by the energy $\hbar\omega$. The increase of γ_S due to quasi-free electron excitation is shown in Figure 9, for a thermal situation. In calculating (19) only electron confinement has been taken into account, neglecting environment effects and, in particular, chemical damping. As a first approximation, we will assume that the relative T_e dependence of g_S is still given by (19) for embedded particles with an effective g_S value extracted by fitting the measured linear absorption spectrum of the studied sample.

The scattering rates of the bulklike processes have not been calculated for an athermal distribution and in the dynamic regime. As a first approximation they can be estimated using the expressions derived for a thermalized system. The T_e dependence of $\Delta\gamma_{e-e}$, computed using the Gurzhi formula:[49,50]

$$\gamma_{e-e}(\omega,T_e) = \frac{\omega^2}{4\pi^2\omega_p}\left[1 + \left(\frac{2\pi k_B T_e}{\hbar\omega}\right)^2\right] \qquad (20)$$

is shown in Figure 9. Although the relative change of γ_S is smaller than the one of γ_{e-e} (Figure 9), the surface term yields an important contribution in small particles where $\gamma_S \gg \gamma_{e-e}$ (for instance, $\gamma_{e-e} \approx 5 \times 10^{-3}$ fs^{-1} in silver and $\gamma_S \approx 5 \times 10^{-1}$ fs^{-1} for $R = 3$ nm). In contrast, γ_{e-ph} is very weakly modified by electron heating and, though it is the main contribution to the room temperature γ, its contribution to $\Delta\gamma$ can be neglected.

On a long time scale, increase of the lattice temperature has also to be taken into account and leads to an increase of γ_{e-ph} due to that of the occupation numbers of the phonons. For T_L larger than the Debye temperature, $\Delta\gamma_{e-ph}$ is proportional to ΔT_L:[49]

$$\Delta\gamma_{e-ph}/\gamma_{e-ph} = \Delta T_L/T_0 \qquad (21)$$

In the equilibrium regime ($T_e = T_L$), the purely electronic mechanisms are almost negligible (since $\Delta T_L \ll \Delta T_e^{me}$), and $\Delta\gamma$ is essentially determined by ΔT_L, in quantitative agreement with the measurements in metal films.[19]

The lattice temperature rise also induces electronic band displacement and warping.[89,90] These can alter both the interband term, via energy band shifts, and the intraband one, via plasma frequency change due to alteration of n_e and m_e. These effects are important in bulk metals, leading in particular to a large decrease of ϵ_1 for frequencies well below Ω_{ib}.[19,43] Similar processes, modified by the confinement, are also expected to contribute to the long delay optical property changes of nanoparticles but, to our knowledge, have not been modeled.

III. Experimental Systems and Samples

All our experiments were performed using a high repetition rate femtosecond pump−probe technique. The pulses were created from the pulse train delivered by a homemade 25 fs Ti:sapphire oscillator tunable in the range 1.07−0.82 μm. Part of the output of the laser was used as the near-infrared pump (some measurements have also been performed by frequency doubling it to directly excite the SPR in Ag). The relative sample transmission change, $\Delta T/T$, was probed in the vicinity either of the silver or gold SPR, or of the silver interband transition threshold. In the former case, probe pulses in the 535−410 nm range were created by frequency doubling the remaining part of the pulse train. In the latter case, UV pulses were generated by frequency tripling it.[20] The two beams were sent into a standard pump−probe setup, with mechanical chopping of the pump beam at 1.5 kHz and differential and lockin detection of ΔT. Taking advantage of the high stability and high repetition rate (76 MHz) of the oscillator, very high sensitivity measurements were performed with a noise level for $\Delta T/T$ in the 10^{-6} range. This sensitivity is essential to study metallic systems in the weak perturbation regime. Furthermore, the excitation process being nonresonant (for a near-infrared pump pulse), it is weakly sensitive to the pump wavelength, and probe

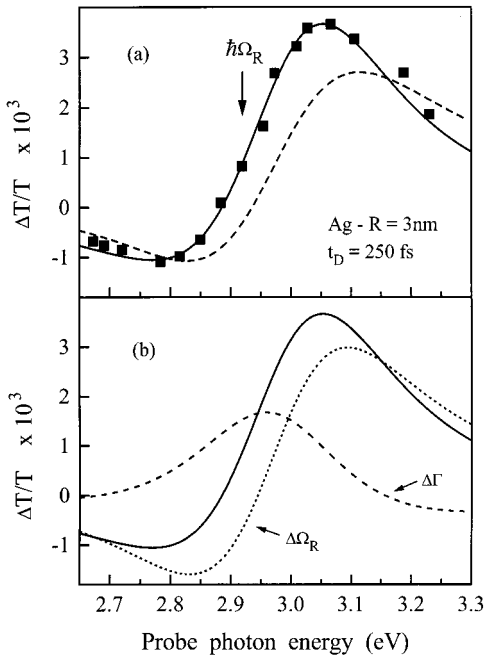

Figure 10. (a) Dispersion of the transmission change around the surface plasmon resonance measured in $R = 3$ nm Ag nanoparticles (Figure 2b) for a pump−probe delay of 250 fs (squares). The full line is a fit assuming a frequency shift $\Delta\Omega_R$ and a broadening $\Delta\Gamma$ of the SPR, and the dashed line, the calculated $\Delta T/T$ dispersion taking into account only the interband term $(\Delta T/T)_b \propto -\Delta\alpha_b$ (Figure 7). (b) Contributions to $\Delta T/T$ due to the SPR frequency shift (dotted line) and broadening (dashed line). The full line is the sum of the two contributions.

wavelength-dependent measurements can be performed by changing the operating wavelength of the Ti:sapphire oscillator.

Most of the experimental investigations described in the following have been performed in spherical silver nanoparticles embedded either in a $50BaO-50P_2O_5$ or in a Al_2O_3 matrix. The former samples were prepared by a fusion and heat treatment technique and the average particle radius R ranges from 2 to 15 nm.[91] The metal volume fraction, p, was in the range 1×10^{-4} to 5×10^{-4} with a sample thickness $L \approx 15$ μm. The latter samples, with $1.5 \leq R \leq 2$ nm, were grown using low-energy cluster beam deposition (LECBD) with co-deposition of alumina.[92] p was typically a few percent with $L \approx 0.2$ μm. We have also performed studies in silver and gold colloids. As confinement induced effects are investigated, narrow size dispersion samples have been used with standard size deviations smaller than 10% of R (measured by TEM).

IV. Surface Plasmon Resonance Dynamics

A. Silver Nanoparticles. As stressed above, the large separation of the interband transition and SPR in silver nanoparticles permits selective investigation of the SPR and electron dynamics.[28,84] We will focus here on the physical origin of the ultrafast nonlinear optical response around the SPR after selective free-electron excitation by a femtosecond pulse. The spectral shape of $\Delta T/T$ measured around Ω_R at a fixed pump−probe time delay exhibits a derivative type of shape, as illustrated in Figure 10. A near-infrared pump pulse has been used here, but identical results were obtained for exciting the SPR. The measured $\Delta T/T$ dispersion is comparable to the $(\Delta T/T)_b$ one, computed by taking into account only the change of the interband part of ϵ (Figure 7). Qualitatively comparing the experimental and theoretical results, one could be tempted to conclude that this is the only contribution here. This is clearly not the case since, for all time delays, both the asymmetry of the spectra of $\Delta T/T$ and the frequency where it changes sign cannot be reproduced by $(\Delta T/T)_b$ (Figure 10). This demonstrates that the intraband term of ϵ is also contributing, i.e., one cannot neglect the electron scattering rate changes (or SPR width change, eq 10).

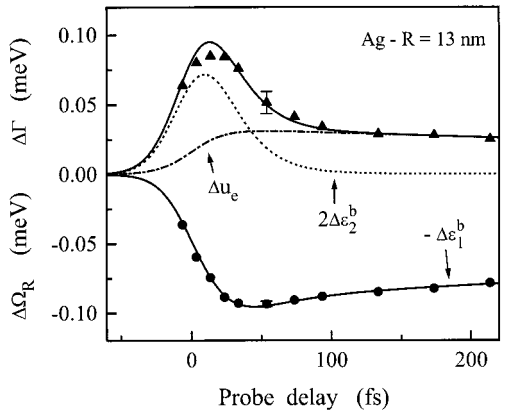

Figure 11. Measured time dependence of the SPR frequency shift $\Delta\Omega_R$ (circles) and broadening $\Delta\Gamma$ (triangles), in $R = 13$ nm Ag nanoparticles in glass. The pump fluence is 100 μJ/cm^2 ($\Delta T_e^{me} \approx 160$ K). The full and dotted lines are the computed $-\Delta\epsilon_1^b$ and $2\Delta\epsilon_2^b$ normalized with the same factor. The upper full line is the estimated full broadening: sum of the interband contribution $2\Delta\epsilon_2^b$ and of the intraband one assumed to be proportional to the electron gas excess energy Δu_e (dash−dotted line).

Taking advantage of the quasi-Lorentzian SPR line shape (eq 9), it is convenient to describe its change in terms of a frequency shift, $\Delta\Omega_R$, and a broadening $\Delta\Gamma$. Using (8) and (10), they are related to $\Delta\epsilon$ by

$$\Delta\Omega_R = -\frac{1}{2}\frac{\Omega_R^3}{\omega_p^2}\Delta\epsilon_1^b(\Omega_R) + \frac{\Omega_R}{\omega_p}\Delta\omega_p \qquad (22)$$

and

$$\Delta\Gamma = \frac{\Omega_R^3}{\omega_p^2}\Delta\epsilon_2(\Omega_R) \approx \frac{\Omega_R^3}{\omega_p^2}\Delta\epsilon_2^b(\Omega_R) + \Delta\gamma \qquad (23)$$

This approach is fully equivalent to the complete one provided that the dispersions of $\Delta\epsilon_1$ and $\Delta\epsilon_2$ are small around Ω_R, which is a good approximation in silver (Figure 7). Using $\Delta T/T = -\Delta\tilde{\alpha}L$ and (9) to link $\Delta\tilde{\alpha}$ to $\Delta\Omega_R$ and $\Delta\Gamma$, a good reproduction of the experimental results has been obtained, as illustrated in Figure 10 (note that A is a constant in eq 9). Actually, the $\Delta T/T$ spectral shape is only sensitive to the ratio $\Delta\Gamma/\Delta\Omega_R$, the $\Delta\Omega_R$ (or $\Delta\Gamma$) value being determined by comparing the computed and measured absolute amplitude of $\Delta T/T$. Note that the short time scale results ($t_D < 0$) cannot be reproduced using this simple approach, based on a generalization of the quasi-equilibrium description of the system optical response, and should be described using a more complete many body model including the real transient nature of the distribution.

The deduced $\Delta\Omega_R$ and $\Delta\Gamma$ exhibit different short time behaviors showing that they reflect different sample property changes (Figure 11). On a longer time scale ($\geq$200 fs) both $\Delta\Omega_R$ and $\Delta\Gamma$ decay exponentially due to electron gas energy losses to the lattice (see section V.B).[28,84]

1. SPR Nonlinear Response: Interband Contribution. For short times, heating of the lattice and the surrounding medium is negligible and the nonlinear response reflects the electron distribution change. The SPR frequency depends only on ω_p and $\epsilon_1^b(\Omega_R)$ (eq 8). n_e, and thus ω_p, being constant for intraband

pumping, $\Delta\Omega_R$ can be related to $\Delta\epsilon_1^b$ (i.e., to the electron induced optical Kerr effect) at the frequency Ω_R (eq 22).

Using the simple model of an isotropic parabolic conduction band and neglecting d-band dispersion, $\Delta\epsilon_2^b$ can be written[93]

$$\Delta\epsilon_2^b(\omega) \propto \frac{\sqrt{\hbar\omega + E_d}}{(\hbar\omega)^2}\Delta f(\hbar\omega + E_d) \tag{24}$$

where $E_d = E_F - \hbar\Omega_{ib}$. $\Delta\epsilon_1^b$ can then be calculated using the Kramers−Kronig relationship, leading to

$$\Delta\epsilon_1^b(\omega) \propto \int \frac{\sqrt{\hbar\omega'}\Delta f(\hbar\omega')}{(\hbar\omega' - E_d)[(\hbar\omega)^2 - (\hbar\omega' - E_d)^2]}\, d\omega' \tag{25}$$

where integration is performed over the perturbed conduction band states. As Ω_R and Ω_{ib} are well separated, one can easily show that for a not too out of equilibrium situation (i.e., for Δf extending over an energy range roughly smaller than $\hbar(\Omega_{ib} - \Omega_R)$ around E_F), $\Delta\epsilon_1^b(\Omega_R)$ is almost proportional to the electron gas excess energy[19]

$$\Delta\epsilon_1^b \propto \Delta u_e(t_D) \propto \int \omega'^{3/2}\Delta f(\hbar\omega', t_D)\, d\omega' \tag{26}$$

This condition is realized after a few tens of femtoseconds (Figure 4). Consequently, $\Delta\Omega_R$ (% $\Delta\epsilon_1^b$) is weakly sensitive to the details of the electron distribution and almost follows the increase and decay of the electron gas energy. This is in agreement with the experimental data and with the results of the model of section II.D.1 (Figure 11).[28,84]

Interband absorption changes can also induce a broadening of the SPR.[28] During and shortly after excitation, the electron distribution is strongly athermal (Figure 4), and interband absorption is induced for frequencies down to $\Omega_{ib} - \omega_{pp} < \Omega_R$ (Figure 4). $\Delta\epsilon_2^b(\Omega_R)$ is then nonzero, leading to a broadening of the SPR (eq 10), which can be interpreted as an induced SPR decay with excitation of a bound d-electron into the conduction band (i.e., SPR decay with single d-electron excitation). The involved final states, around $E_f = E_F - \hbar(\Omega_{ib} - \Omega_R)$, are well below E_F and return to equilibrium on a few tens of femtoseconds by e−e scattering.[15,73−78] Consequently, this additional SPR relaxation channel decays very quickly in silver (where $E_f \approx E_F - 1$ eV and $\tau_{e-e}(E_f) \approx 20$ fs[74,75]) and is thus at the origin of the observed transient induced SPR broadening (Figure 11).

It is important to note that the amplitude of the interband contribution to $\Delta\Omega_R$ and $\Delta\Gamma$ are linked (eqs 22 and 23) since $\Delta\epsilon_1^b$ and $\Delta\epsilon_2^b$ are linked by the Kramers−Kronig relation, but $\Delta\Omega_R$ depends on the Δf change over the full electron energy range while $\Delta\Gamma$ depends only on its local value (around E_f).

2. SPR Nonlinear Response: Intraband Contribution. On a longer time scale ($t_D \geq 50$ fs), $\Delta\epsilon_2^b(\Omega_R)$ is negligible and the long delay broadening $\Delta\Gamma$ has been ascribed to alteration of the intraband electron scattering processes, i.e., increase of γ (eq 18, with $\Delta\Gamma \approx \Delta\gamma$ for $t_D \geq 50$ fs, eq 23). Information on the electron distribution dependence of the electron interactions in a confined metallic system can thus be obtained.[28,84]

On a short time scale, both the e−e and electron−surface scattering rates significantly contribute and one can write $\Delta\Gamma \approx \Delta\gamma_{e-e} + \Delta\gamma_S$ (section II.D.2). Their relative contributions can be separated by measuring $\Delta\Gamma$ as a function of the nanoparticle size since the $\Delta\gamma_S$ amplitude is inversely proportional to R (eq 18) while $\Delta\gamma_{e-e}$ weakly varies with R (at least for $R \geq 3$ nm[84]). As ΔT_e^{me} depends on the nanoparticle size for the same pump fluence, the induced broadening in the different samples were compared after normalizing them to the frequency shift $\Delta\Omega_R^0$ for a fixed probe delay t_0 ($\Delta\Omega_R^0$ is actually used as a measure of the excitation amplitude[28]). The results obtained for $\Delta\Gamma$ measurements performed for a probe time delay of 300 fs show a linear dependence of $\Delta\Gamma/\Delta\Omega_R^0$ on $1/R$, in agreement with (18) (Figure 12). This shows that the surface mechanism importantly contributes to $\Delta\Gamma$ and even becomes dominant for the smallest nanoparticles, the ratio of the surface to the bulk-like contributions rising from ∼1 for $R = 13$ nm to ∼4 for $R = 3$ nm.[28,84] This surface contribution is actually a manifestation of the quantum confinement in the nanoparticle nonlinear response.

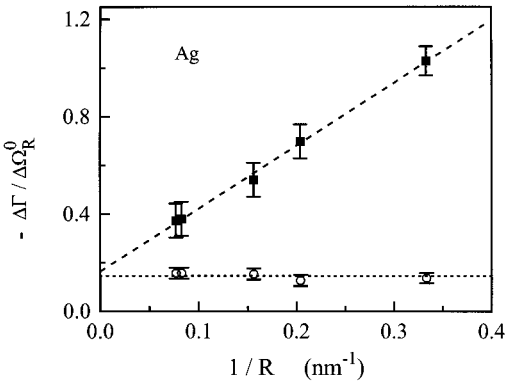

Figure 12. Measured SPR broadening $\Delta\Gamma$ for a probe delay $t_D = 300$ fs (squares) and 2 ps (open circles) normalized to the SPR shift $\Delta\Omega_R^0(R)$ at $t_D = 300$ fs in Ag nanoparticles embedded in glass as a function of their inverse radius ($1/R$).

For longer delays, the electron temperature strongly decreases, approaching the lattice one, and the residual broadening is then dominated by an increase of the e−ph scattering rate due to increase of T_L: $\Delta\Gamma \approx \Delta\gamma_{e-ph}$ (section II.D.2). Consequently, the long time delay broadening is expected to be almost independent of the nanoparticle size (except for a possible change of the e−ph scattering efficiency for small sizes, section V.B), in very good agreement with the experimental data (Figure 12).

3. Comparison with Bulk Materials. It is interesting to compare the measured optical response in nanoparticles to that of metal films (that are identified to bulk materials) for the same excitation and probing conditions. The transient dielectric constant changes, $\Delta\epsilon_1$ and $\Delta\epsilon_2$, of an optically thin film can be determined by simultaneously measuring $\Delta R/R$ and $\Delta T/T$.[19,20,94] In bulk silver, the interband term dominates the short time scale (few picoseconds) response around Ω_R,[20] and the measured $\Delta\epsilon$ can thus be directly compared to $\Delta\epsilon^b$ computed using the model of section II.D.1. The band structure model of Rosei has been shown to yield a qualitative reproduction of the measured data but leads to an underestimation of $\Delta\epsilon_2$.[20] This is due to the fact that this model is only valid for probing close to the interband transition threshold. For strongly athermal distributions and probing off resonance, it underestimates the involved density of states. Conversely, the simple model of undispersed d-bands and parabolic isotropic conduction band leads to an overestimation of $\Delta\epsilon_2$, due to overestimation of the joint density of states.[20] A quantitative reproduction of the amplitude of both $\Delta\epsilon_2$ and $\Delta\epsilon_1$ (linked by the Kramers−Kronig relation) is obtained by phenomenologically averaging the results of the two band structure models (Figure 13).

Using the same approach a quantitative reproduction of both $\Delta\Omega_R$ and short time scale $\Delta\Gamma$ is obtained in nanoparticles (Figure 11). The same normalization factor has been used for

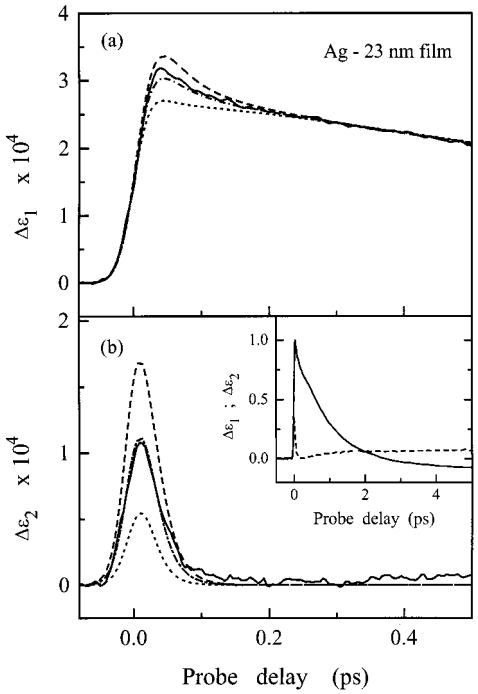

Figure 13. Measured time-dependent changes of the real (a) and imaginary (b) parts of the dielectric function at $\hbar\omega_{pp} \approx 2.9$ eV in a 23 nm Ag film (full lines) for $\hbar\omega_{pp} \approx 1.45$ eV and $= \Delta T_e^{me}$ 18 K. The inset shows the same results on a longer time scale. The dotted and dashed lines are the interband terms ($\Delta\epsilon_1^b$ and $\Delta\epsilon_2^b$ normalized using the same factor), computed using the Rosei's and parabolic band structure models, respectively, and the dash−dotted line is their average.

comparing $\Delta\Omega_R$ to $-\Delta\epsilon_1^b$ and $\Delta\gamma_b$ to $2\Delta\epsilon_2^b$ (see eqs 22 and 23). $\Delta\epsilon^b$ computed using the bulk parameters have been used here since the electron dynamics is weakly modified by confinement in $R = 13$ nm particles. This agreement confirms that the SPR frequency shift and short time delay broadening are due to alteration of the interband properties, which exhibit similar behaviors in films and nanoparticles.

After this transient contribution ($\Delta\epsilon_2^b(\Omega_R) \approx 0$ for $t_D \geq 100$ fs), $\Delta\epsilon_2$ is almost 0 for $t_D = 100$ fs and rises with τ_{e-ph} (i.e., with T_L) in films due to the increase of $\Delta\epsilon_2^f$, i.e., $\Delta\gamma_{e-ph}$ (Figure 13). In contrast, in nanoparticles, $\Delta\Gamma$ (and thus $\Delta\epsilon_2$) exhibits a finite value decaying with τ_{e-ph} (Figure 11). A very good reproduction of $\Delta\Gamma$ can be obtained by linearizing the response assuming that $\Delta\gamma$ (and thus $\Delta\epsilon_2^f$) is proportional to Δu_e (Figure 11). This different behavior of films and nanoparticles indicates that the scattering rate changes related to the electron temperature are larger in the latter, which is consistent with a large contribution from electron−surface scattering.[84] Acceleration of e−e interactions due to confinement can also play a role for small particles, $R \leq 5$ nm typically (section V.A).

B. Gold and Copper Nanoparticles. In the case of gold and copper nanoparticles, the SPR frequency is very close to Ω_{ib}, making separation of the interband and intraband effects difficult since, in contrast to silver, the interband term $\Delta\epsilon^b(\Omega_R)$ contributes to both the real and imaginary parts of $\Delta\epsilon(\Omega_R)$ for any time delays (Figure 8). Furthermore, the linear absorption spectrum around the SPR cannot be simply described by a quasi-Lorentzian shape and the general expression (9) linking the absorption to ϵ has to be used for modeling $\Delta\tilde{\alpha}$. Consequently, although the line shape of the computed interband contribution $\Delta\alpha_b$ suggests a simple broadening effect, its interpretation is much more complex and has to take into account both the dispersion of $\Delta\epsilon_1^b$, $\Delta\epsilon_2^b$ and of the enhancement of the nonlinear response around the SPR (Figure 8).

The transient responses of gold nanospheres embedded in a glass matrix and in solution have been investigated mostly in the strong excitation regime.[23,25,26,29−31] In both systems, the transient $\Delta T/T$ line shapes are in qualitative agreement with the ones predicted by taking into account only the intraband term (Figure 8). We have also recently observed a very similar response in gold colloids in the weak perturbation regime. These results show a dominant contribution from the interband term in both regimes[26,31,81,95] and a weak influence of the electron scattering rate increase (i.e., of the intraband term). This is consistent with the results in silver where the former contribution dominates whenever it is present (i.e., for short time delays for $\Delta\Gamma$).

The measured line shapes are, however, always slightly broader than the computed ones. A similar discrepancy has been observed in CW thermomodulation measurements and femtosecond investigations of gold films.[15,87,88] It can be ascribed to oversimplification of the band structure by the Rosei's model (interband transition resonant effects being observed here, the spectral shape of the computed response is very sensitive to the band structure model) and neglecting of the width γ_{ib} of the interband transitions (due to conduction electron scattering and d-hole lifetime).[22,94,96] In the case of silver, this last correction is negligible since off-resonant conditions are realized when probing around the SPR.

Similar transient spectral responses have been reported in the case of copper nanoparticles,[21,22] consistent with their similar linear absorption spectra. However, a probe wavelength dependence of the measured dynamics around the SPR has been reported for small sizes in Cu[22] and ascribed to an increase of γ_{ib} due to enhancement of the e−e Coulomb interaction when an energy close to the SPR energy is exchanged.[97,98] This enhancement is similar to the one computed in bulk semiconductors when treating screening in the plasmon pole approximation,[99] but its amplitude is here strongly size-dependent. A qualitative reproduction of the data has thus been obtained, assuming instantaneous internal thermalization of the electron gas.[97] Quantitative comparison is, however, difficult since it requires inclusion of the electron internal thermalization dynamics and of a more detailed band structure model.

V. Electron Relaxation in Metal Nanoparticles

Femtosecond techniques have been extensively used to analyze the elementary electron scattering processes in bulk metals.[13−20,73−78] We will discuss here their extension to the investigation of the impact of the confinement on e−e and e−ph interactions in metal nanoparticles.

A. Electron−Electron Scattering. Electron−electron scattering and the correlated internal thermalization dynamics of the conduction electrons have been investigated in gold and silver films by taking advantage of the sensitivity of the absorption around the interband transition threshold Ω_{ib} on the electron distribution close to E_F (Figure 2a, inset). Electron internal thermalization is accompanied by a buildup of the occupation number change Δf around E_F (Figure 4). The interband part of the absorption change around Ω_{ib} is thus very sensitive to the thermal or athermal character of the distribution[15,20] and thus yields information on its evolution to a Fermi−Dirac distribution (i.e., establishment of the electron temperature, T_e).

The situation is similar in silver nanoparticles where absorption around Ω_{ib} is almost unaffected by confinement (for $R \geq 1.5$ nm), and in particular, not influenced by the SPR (Figure

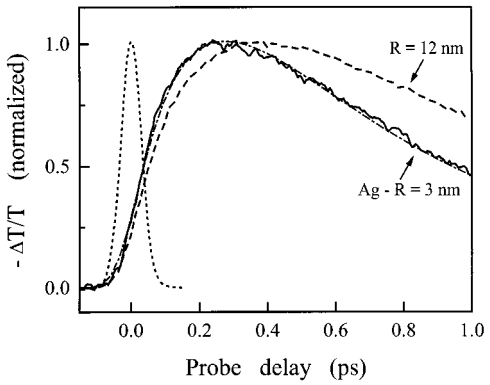

Figure 14. Time behavior of the transmission change $-\Delta T/T \propto \Delta\tilde{\alpha}L$ measured for $\hbar\omega_{pp} \approx 3.95$ eV and $\hbar\omega_{pp} \approx 1.32$ eV in $R = 12$ nm (dashed line) and 3 nm (full line) Ag nanoparticles in glass. The dash−dotted line is a fit for the $R = 3$ nm case using (27) and the dotted line the pump−probe cross-correlation.

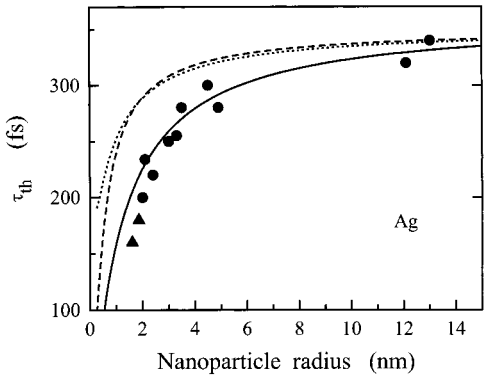

Figure 15. Size dependence of the electron thermalization time τ_{th} for Ag nanoparticles in a $BaO-P_2O_5$ (dots) and Al_2O_3 (triangles) matrix. The full line shows the computed τ_{th} taking into account both the spillout and d-electron localization effects, and the dashed and dotted lines show their respective contributions.

2a). As in films, the interband term dominates the response in this spectral range, permitting us to follow the internal thermalization dynamics and to compare it for different particle sizes (Figure 7). The measured spectral shape of $-\Delta T/T \propto \Delta\tilde{\alpha}$ has been found to be in very good agreement with the computed one and, in particular, exhibits a maximum around $\hbar\omega_{pr} \approx 4$ eV.[32] Using the same procedure as in films, a characteristic internal thermalization time τ_{th} has been defined by fitting the measured signal around 4 eV, assuming a monoexponential rise and using a response function of the form[15,20,79]

$$u(t) = H(t)[1 - \exp(-t/\tau_{th})] \exp(-t/\tau^0_{e-ph}) \qquad (27)$$

where $H(t)$ is the Heaviside function (Figure 14). The exponential decay with the time τ^0_{e-ph} stands for electron energy transfer to the lattice.[28] For $R \geq 5$ nm, τ_{th} is close to its film value ($\tau_{th} \approx 350$ fs[20]) and strongly decreases for smaller sizes (Figure 15). Comparable results were obtained for nanoparticles embedded either in a $50BaO-50P_2O_5$ or in a Al_2O_3 matrix (Figure 15) or deposited on a substrate, showing that the results are independent of the environment and sample preparation method. Furthermore, no dependence of the time response on the pump fluence or pump photon energy has been observed, as expected for a weak perturbation. The τ_{th} decrease with R thus demonstrates an intrinsic confinement induced fastening of the electron−electron energy exchanges.[32]

A similar approach has been used in gold colloids by El-Sayed et al.[81,31] The measured $\Delta\alpha_b$ also exhibits a delayed rise around Ω_{ib} with the additional complication due to overlapping of the SPR and interband responses (Figure 8). The τ_{th} values measured for $R = 4.5$ and 24 nm[81] are almost identical to the bulk one ($\tau_{th} \approx 500$ fs[15]). This absence of variation in this size range is consistent with the silver results.

The τ_{th} size dependence has been ascribed to surface-induced modification of the electron environment in a nanoparticle as compared to the bulk.[32] In particular, it has been shown that the wave functions of the conduction electrons extend beyond the particle radius defined by the ionic lattice (electron spill-out[100]). This leads to a reduction of their density n_e and thus of ω_p that manifests itself by a red shift of the SPR with size reduction in alkali metal clusters.[101] Conversely, the d-electron wave functions are localized in the inner region of the particle, leading to an incomplete embedding of the conduction electrons in the core electron background.[102] Both effects lead to less efficient screening of the e−e Coulomb interactions close to a surface in noble metals and are thus expected to increase the effective e−e scattering rate in small nanoparticles.

Assuming static screening, the dependence of the scattering time of an electron out of its state on n_e and core electron screening amplitude (related to $\epsilon_{sc} = \epsilon_1^b(0)$) in the bulk metal is given by[103]

$$\tau_e \propto n_e^{5/6} \epsilon_{sc}^{1/2} \qquad (28)$$

For a weak perturbation, τ_{th} is proportional to τ_e[20] and as a first approximation, the global scattering rate in a nanoparticle has been estimated by averaging τ_e^{-1} over the particle volume using position-dependent n_e and ϵ_{sc}.[32] Although this local approach is a crude approximation, it is partly justified by the short screening length of the Coulomb interaction (of the order of the inverse of the Thomas−Fermi wave vector, ~1 Å in metals).

The spatial variations of ϵ_{sc} and n_e in silver clusters were previously quantitatively modeled to analyze the size dependence of the surface plasmon resonance frequency.[66] The d-electron surface exclusion effect was described using a phenomenological two-region dielectric model, where screening by the d-electrons is effective only in a core sphere of radius $R_c = R - c$ with $c = 3.5$ au (i.e., $\epsilon_{sc} = \epsilon_{sc}^{bulk}$ inside the core sphere and $\epsilon_{sc} = 1$ outside).[66,102] n_e was calculated using the jellium dielectric sphere model.[66,100] Using this model, a good reproduction of the experimental τ_{th} size dependence has been obtained with similar contributions from the two screening reduction effects (Figure 15). It actually essentially reflects the increasing percentage of electrons in the perturbed surface layer (about 25% of the electrons are out of the R_c radius core sphere for $R = 2$ nm), i.e., the increasing influence of the surface in small clusters. This enhanced e−e scattering close to the surface is consistent with the larger dephasing times measured for surface than for bulk electrons.[104]

Although a good reproduction of the data is obtained, a systematic deviation is observed for small sizes ($R \leq 2$ nm). The above model, based on a simple extension of the bulk calculations, overlooks specific features of the confined materials. In particular, the e−e scattering rate has been derived using the bulk electron wave functions and includes momentum conservation. This is relaxed in confined systems, due to, classically, electron scattering off the surfaces, leading to opening of additional e−e scattering channels and thus further size-dependent modifications of the e−e interactions (this effect is comparable to the increase of the electron optical scattering rate due to surface effects, eq 4). A more correct description requires nonlocal calculations of the e−e scattering rate and

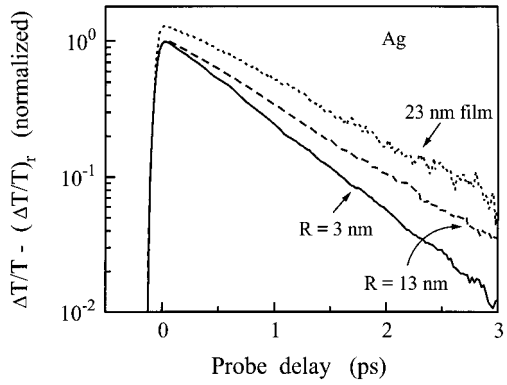

Figure 16. Time-dependent transmission change measured for $\hbar\omega_{pp} = 2.97$ eV in $R = 3$ and 13 nm Ag nanoparticles in glass and in a 23 nm Ag film on a logarithmic scale (the latter has been upshifted for clarity). $(\Delta T/T)_r$ is the small residual change (smaller than 10% of the maximum amplitude) measured for a long delay ($t_D \geq 15$ ps).

many-body effects in a nanoparticle using the confined electron wave functions.

B. Electron−Lattice Coupling. The transient signals measured in metallic systems decay in a few picoseconds with the electron gas excess energy and thus contain information on the energy exchanges of the electrons with their environment. In the case of films, this is essentially limited to the metal lattice, permitting direct measurement of the electron−phonon interaction time (i.e., the energy transfer time as defined using the two-temperature model, eq 14). For nanoparticles the electron energy can also be damped to the surrounding solvent or matrix either directly or via the metal lattice possibly modifying the observed relaxation.

Many time-resolved investigations have been performed to analyze electron−lattice coupling and its modification by the confinement in noble metal nanospheres and nanorods (Ag[23,27,28,84,94,105,106] Au,[23,25,26,29−31,80,81,107,108] Cu,[21,22] and Ag−Au alloys[31]) in different matrices or solvents, in gold nanoshells,[109] and in Ga,[24] Sn,[110] Pt,[23] and Na[111] nanoparticles. There is, however, a large scattering of the reported decay times for the same metal.[13] As most of the experiments were performed in the strong excitation regime, these discrepancies can be partly ascribed to the perturbation-dependent slowing down of the electron gas cooling (section II.B). This is confirmed by the results of systematic pump-power-dependent measurements performed in the case of gold,[29,31,82] copper,[21] and silver[27,94] nanoparticles that clearly show a large increase of the observed decay time τ_{e-ph} with the pump power. The intrinsic low perturbation values, τ^0_{e-ph}, of τ_{e-ph}, and thus the e−ph coupling constants $G = C_e(T_0)/\tau^0_{e-ph}$ (eq 14), inferred by these systematic studies are consistent with the ones reported in films.[15−17,20,112]

As outline above, the intrinsic energy exchange time τ^0_{e-ph} can be directly determined in the weak perturbation regime (section II.B). In agreement with the two-temperature model (14), an exponential decay of the transmission change has then been observed, as illustrated in Figure 16 for silver. As in metal films, a deviation from an exponential behavior can be observed up to ~500 fs due to the athermal character of the distribution[19] but will not be discussed here. Measurements performed in Ag for R ranging from 2.1 to 15 nm have shown that τ^0_{e-ph} is comparable to its bulk value ($\tau^0_{e-ph} \approx 0.85$ ps) for large nanoparticles ($R \geq 5$ nm, typically) but significantly decreases for smaller ones (with $\tau^0_{e-ph} \sim 0.6$ ps for $R = 2.1$ nm).[84] In contrast, using extrapolation of the strong perturbation measurements, no size dependence of τ^0_{e-ph} (or G) has been estimated in the case of gold colloidal nanoparticles with radii between 1.2 and 50 nm by the Hartland group.[30,82] A similar conclusion was drawn by the El-Sayed group for radii ranging from 1 to 25 nm.[31,80,81] A nonmonotonic size dependence has been observed by Zhang et al. in gold[107] with possible modification of the decay time due to strong excitation.

A decrease of the $\Delta T/T$ decay time with R has also been reported in tin[109] and gallium[24] nanoparticles for radii ranging from 2 to 6 nm and 5 to 9 nm, respectively. The size dependence is, however, much larger than for silver, τ_{e-ph} being almost proportional to R over the investigated range. This variation has been interpreted in terms of electron coupling with the surface acoustic modes of the particles (i.e., the quantized vibration modes replacing the bulk ones, section VI) and quenching of the electron−bulk phonon interactions using the Belotskii and Tomchuk model.[113,114] However, this model, only applicable to small sizes, predicts a much slower electron−lattice energy transfer than in the bulk,[114] in contrast to the observations in noble metals.

The origin of the different behaviors observed by the different groups and the actual size dependence of the electron−lattice energy exchanges is not yet clear, although the observation of a τ^0_{e-ph} size dependence in silver similar to that of τ_{th} suggests a confinement-induced acceleration of these exchanges due to increase of the electron−lattice mode coupling, as in semiconductor nanoparticles.[115] An important point here could be the influence of the environment,[23,46,106] and of the interface layer and quality (as has been observed for the SPR width[57]). This can be particularly important for small sizes for which the particles are strongly coupled with their environment, the ratio of the surface to volume atom numbers strongly increasing as R decrease. Actually, the decay times measured in 9 nm gold particles have been shown to depend on the solvent (water or cyclohexane).[23] Similarly, relaxation has been found to be faster in Ag particles embedded in aluminate than in silica glass.[106] Though both of these measurements were performed in the strong excitation regime, similar matrix effect could affect the weak perturbation studies. An important effect could be local heating of the matrix around the nanoparticles with thus a strong influence of the thermal conductivity of the matrix material.[46] Additional experimental and theoretical investigations are clearly needed to understand electron−lattice coupling in confined metallic systems.

VI. Vibrational Dynamics

The vibrational ionic motion in bulk materials is described in terms of phonons. This approach assumes translational invariance and can be used only if the system size is much larger than the spatial extension of the considered phonon, i.e., typically, its wavelength λ_{ph}. For smaller sizes, the phonons are sensitive to the presence of interfaces and the eigenmodes must satisfy new boundary conditions: the vibrational modes are then quantized. For acoustic modes, the low-frequency phonon spectrum, associated with long wavelengths, is first altered with the appearance of discrete acoustic vibration modes, while the high-frequency (i.e., small wavelength with $\lambda_{ph} \ll R$) phonons are almost unaffected.[116−122] The quantized mode properties, frequency and damping, reflect the size, shape, and environment of the particles. Their investigation can thus bring important information on the composite material and, in particular, on the important problem of particle−matrix energy transfers, which is essential for the development of practical devices.

A. Vibrational Properties of Nanoobjects. For not too small nanoobjects (typically $R \geq 1$ nm for a sphere) the low-frequency

modes, associated with a spatial displacement on a scale much larger than the interatomic distance, can be described as the vibration eigenmodes of a homogeneous body.[116−121] This corresponds to a "macroscopic" description of the particle neglecting its atomic structure[123,124] and overlooking the real nature of the interface. The acoustical mode properties then only depend on the density and elastic constants, assumed isotropic, of the particle material and of its environment.[120] The eigenmodes can then be divided into spheroidal and torsional vibrations, corresponding to oscillations with and without volume change, respectively.[121] Because of the isotropy of the excitation process, only the former are observed in time-resolved experiments.[42] The fundamental radial mode of a sphere corresponds to its isotropic expansion and contraction (breathing mode) with a complex frequency inversely proportional to R:

$$\tilde{\omega}_0(R) = \xi_0 v_L^{(s)}/R \tag{29}$$

where $v_L^{(s)}$ is the longitudinal sound velocity in the sphere and ξ_0 the normalized frequency. For a weak coupling with the matrix, i.e., a large mismatch of the acoustical impedances $Z^{(m),(s)} = \rho^{(m),(s)} v_L^{(m),(s)}$ of the matrix (m) and sphere (s) materials, the eigenfrequency ω_0 can be defined as the real part of $\tilde{\omega}_0$[120] and is weakly sensitive to the environment (with $\mathrm{Re}(\xi_0) \sim 3$ in Ag).[42] In contrast, the damping rate γ_0, defined as the imaginary part of $\tilde{\omega}_0$, is nonzero only in the presence of a matrix. It reflects expansion of the spherical wave around the sphere[120] and is thus obviously very sensitive to the nature of the environment (presence of an interface layer, solvent, type of glass, ...).

The frequency of the vibrational modes of metal and semiconductor nanoparticles have been studied using spontaneous Raman scattering[125−128] but no information has been obtained on their damping. This is difficult to address in the spectral domain, especially in the case of metallic systems, because of the low frequency and large damping of these modes. Time-resolved optical investigations have been recently reported in semiconductor[129,130] and metal nanospheres,[29,30,39,41−43,131] nanoellipsoids,[132] and core−shell spheres,[133] yielding information not only on the frequency but also on the damping of the breathing mode.[41,130]

B. Coherent Vibrational Oscillations. Direct time domain observation of coherent vibrational motions has been reported in many different bulk and confined systems.[134−144] In these experiments, a vibration mode is triggered on a much shorter time scale than its oscillation period by a femtosecond pulse and its subsequent motion is followed by monitoring the induced system optical property modulation.[134−136] In the case of nanoparticle material, excitation is coherent in the sense that the particles are excited and subsequently oscillate in phase.

In metal nanoparticles, one can take advantage of the enhancement of the nonlinear response in the vicinity of the SPR to detect these oscillations.[41] These show up as oscillations of $\Delta T/T$ on a few picosecond time scale, superimposed on a slowly decaying background. The latter is a consequence of the induced temperature rise of the thermalized particle and decays in a few hundred picoseconds by heat diffusion to the matrix. The oscillations actually reflect modulation of the SPR frequency by the breathing mode (Figure 17):[41−43] the electronic properties of each nanosphere adiabatically follow the lattice expansion and contraction, leading to a modulation of the real part of the metal particle dielectric function (and thus of Ω_R (eq 8)), consistent with the results obtained for the expansion mode of metal films.[43]

Within the experimental accuracy, the measured oscillation frequency has been found to be in good agreement with the calculated breathing mode frequency in all the investigated systems (Figure 18, eq 29), showing that this mode dominates the time response.[40,41] This mode selectivity has been attributed to the isotropy of the excitation process mediated by lattice expansion.[42] In this mechanism, energy is first selectively injected in the electron gas and subsequently transferred to the lattice, in a time scale of the order of $\tau_{e-ph} \sim 1$ ps. Because of lattice anharmonicity, this fast heating of the lattice displaces the equilibrium radius, R_{eq} of the spheres (i.e., an expansion

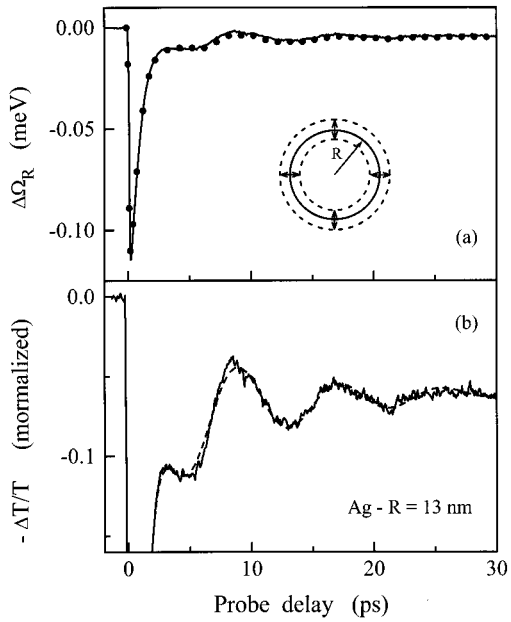

Figure 17. (a) Time dependence of the SPR frequency shift $\Delta\Omega_R$ (circles) measured in $R = 13$ nm Ag nanoparticles in glass. The full line is the normalized $\Delta T/T$ for $\hbar\omega_{pp} = 2.85$ eV. The inset is a sketch of the breathing movement of the nanospheres. (b) Same transmission change $-\Delta T/T \propto \Delta\Omega_R$ on an enlarged scale. The dashed line is calculated for a lattice mediated displacive excitation (30).

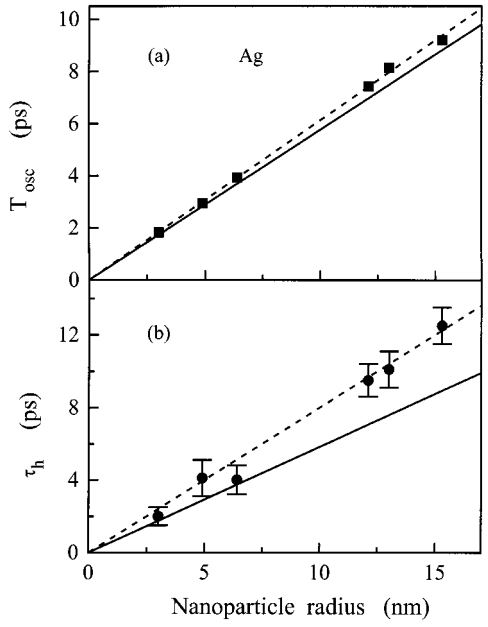

Figure 18. (a) Measured oscillation period T_{osc} as a function of the Ag nanoparticle radius. The lines show the computed period $2\pi/\omega_0$ of the breathing mode for free (dashed line) and $BaO-P_2O_5$ (full line) embedded Ag nanoparticles. (b) Measured homogeneous damping time τ_h as a function of R. The dashed line is a fit and the full line the damping time $\tau_0 = 1/\gamma_0$ computed for a perfect nanoparticle−matrix contact.

would be induced in the fully thermal situation) much faster than the breathing mode period (or equivalently the sphere expansion or surface movement characteristic time). Their radii start increasing simultaneously and subsequently oscillate around their new equilibrium value: the breathing mode is impulsively launched with a well-defined phase.

The average oscillation amplitude is related to R_{eq} (i.e., to the observed background amplitude), but its actual value in one particle depends on the number of photon, N_{phot}, it has absorbed. This is similar for a large value of N_{phot}, i.e., for large R (with on the average $N_{phot} \approx 200$ for a $R = 13$ nm Ag particle and a pump fluence of 100 μJ/cm^2 at $\hbar\omega_{pp} = 850$ nm), but can be very different for smaller sizes (with on the average $N_{phot} \approx 0.4$ for a $R = 1.6$ nm Ag particle in the same conditions, i.e., most of the particles are unexcited).

Assuming the particle contributions to be independent, the indirect displacive excitation process can be described using a damped harmonic oscillator. The oscillation amplitude is then solution of[41]

$$\ddot{x} + 2\frac{\dot{x}}{\tau_0} + {\omega_0}^2\{x - x_0[1 - \exp(-t/\tau_{e-ph})]\} = 0 \quad (30)$$

where x_0 is the new equilibrium position. Using this approach, a very good description of both the phase and amplitude of the oscillations have been obtained for large Ag nanoparticles ($R \geq 10$ nm) in the weak perturbation regime (Figure 17, with $\tau_{e-ph} = \tau^0_{e-ph}$). Note that the amplitudes of the oscillations and of the residual background are simultaneously reproduced.[43] Similar agreement has been demonstrated in the case of gold colloids with an observed phase shift when the pump fluence is increased, consistent with (30) when taking into account slowing-down of the electron lattice energy exchanges in the strong perturbation regime using an effective τ_{e-ph} value.[30]

For small Ag particles, direct coupling with the nonequilibrium electrons has been shown to also significantly contribute.[42] This mechanism, related to the electron contribution to the lattice dilation,[145] is also isotropic and can be described by introducing a transient force in (30), rising with energy injection by the pump pulse and decaying with its transfer to the lattice.[138−140] Its dynamics is different from the indirect mechanism one (which corresponds to application of a long lasting force), and its influence has been studied by analyzing the phase of the oscillations.[41,42] As expected, the role of the direct process has been found to increase with decreasing the mode period (or, equivalently, R) due to decrease of its transient character. This second mechanism also contributes to the excitation of the breathing modes of large Ag ellipsoids for very large energy injection ($\Delta T_e^{me} \approx 3000$ K).[132]

C. Breathing Mode Damping. A single mode dominating the time domain response, its intrinsic damping, τ_h, can be determined from the oscillation damping.[41] One has, however, to take into account the size dispersion of the excited nanoparticles since, because of their slightly different breathing mode frequencies, they drift out of phase with time and their contributions eventually destructively interfere. This inhomogeneous damping can be taken into account by summing up the individual contributions of the nanoparticles using the TEM measured sample size distribution. For narrow size dispersion nanoparticles embedded in a glass matrix, the intrinsic damping is sufficiently large to dominate the measured relaxation and τ_h can thus be determined.[41] The results obtained in the case of Ag nanospheres show that τ_h is proportional to R (Figure 18), in agreement with (29). This dependence is a simple consequence of the energy transfer from the sphere to the matrix, τ_h being proportional to the ratio between the elastic energy in the sphere volume and the energy flow rate through the surface, and thus to R.

The experimental values of τ_h are, however, significantly larger than the theoretical ones calculated assuming the metal−glass interface to be perfect (i.e., a perfect continuity is assumed), which is not the case in practical situation (Figure 18). This discrepancy has been ascribed to metal−glass interface defects and/or the existence of an interface layer that negligibly influence the frequency of the breathing mode,[117,118] but decrease its coupling to the matrix.[41] This sensitivity of τ_h on the metal−matrix interface quality could be exploited to test nanoparticle fabrication procedures and sample quality.

The situation is different for a softer environment, as in the case of colloids, where, because of the large acoustic mismatch between the metal and the surrounding medium, the intrinsic damping is much weaker. A good correlation between the apparent damping time and the measured size distribution has then been obtained, showing that the inhomogeneous contribution dominates the oscillation decay.[29,30]

D. Acoustic Mode Optical Control. From a general point of view, if it is possible to impulsively launch a material mode, it is also possible to control its amplitude using a multiple excitation scheme. This is also the case for the ensemble of local oscillators formed by the nanoparticles whose mechanical movement can thus be optically controlled.[43] This has been demonstrated for $R = 13$ nm Ag nanospheres in the simplest situation of two pump-pulses delayed by half the oscillation period, $\Delta t_{pump} = T_{osc}/2$: expansion of the spheres is launched by the first pulse and stopped by the second one.

Note that this simple description in terms of single particle movement is only valid if all the observed particles are excited in a similar way. This is about the case for the investigated large particles ($R = 13$ nm), each of them absorbing a large number of photons N_{phot}, and their movement being on the average stopped. If only a fraction of particles are excited (for small R), the disappearance of the $\Delta T/T$ oscillation is then essentially due to excitation of a second class of particles that oscillate out of phase with the first ones, and not to single particle oscillation stopping. For large particles, this multiple excitation scheme offers the possibility of manipulating the acoustic waves in these systems.

VII. Conclusions and Perspectives

Time-resolved experiments have emerged as powerful tools for the selective investigation of electron interaction processes and their modification by confinement in metal nanoparticles. Results have now been obtained on electron−electron and electron−phonon scattering in noble metal particles over very large size ranges and for different types of environment. Electron−electron energy exchanges have been shown to be almost unaffected by confinement for sizes larger than 10 nm (i.e., nanospheres of radius larger than 5 nm) and to strongly increase for smaller sizes. Extension of these first measurements to other metals or types of confinement (1D or 2D systems) and the use of other techniques, such as time-resolved photoemission,[146] would be particularly interesting here. The size dependence of electron−lattice energy exchanges is still controversial. A possible origin of the discrepancy between the results reported by the different groups could be the strong influence of the surrounding media and/or difficulty of comparing experiments performed in very different conditions. Further systematic investigations are clearly necessary, in particular as a function of the environment. This point is also very important

for the damping of the coherent acoustic breathing mode of the nanoparticles, which is very sensitive to the nature of the surrounding media and interface quality. This is related to the general and central problem of energy and charge exchanges at a heterogeneous interface, whose understanding is essential for the engineering and applications of these systems.

On the theoretical side, the electron dynamics modeling is based on a small solid approach, i.e., modifications are introduced to the bulk material response. This is justified for not too small nanoparticles, formed by more than a few hundred atoms, for which quantum mechanical confinement only introduces correction to their properties, but only constitutes a first approximation. Calculation of the different electron scattering rates using a quantum mechanical approach would be very interesting here and is necessary for understanding electron interactions in a confined system and evolution from a bulk to a molecular behavior. Extension of these experimental and theoretical studies to smaller systems should bring important information on the impact of confinement on electron interaction processes in reduced dimensionality systems.

The ultrafast optical nonlinearity around the surface plasmon resonance is directly related to the electron distribution change and to its dynamics. Modification of the interband contributions to the dielectric function concomitant with change of the interband absorption spectrum due to Fermi surface smearing is a very important effect whenever it is present. The intraband contribution also plays an important role in the case of silver where the surface plasmon resonance is well separated from the interband transitions. In particular, increase of the electron−surface optical scattering rate with heating of the electron gas has been found to importantly contribute to small nanoparticle optical nonlinearity. This surface-induced mechanism is specific to confined systems and is a manifestation of quantum confinement in the nonlinear response.

Up to now all the experimental studies were performed on an ensemble of nanoparticles (few tens of thousand to one million, typically) and the responses are thus averaged over their size distribution and environment fluctuation. Linear spectroscopy of individual metal nanoparticles using near field optical microscopy has been recently reported.[147] Extension of these techniques to the time domain, as was done in the case of semiconductor wires[148,149] would bring new insight into the understanding of the physics of these systems. On the other hand, most of the measurements were performed in dilute material so that particle coupling can be neglected. High density and, in particular, self-organized nanoparticle systems can now be grown and exhibit collective properties.[12,150−153] Study of the impact of this coupling on their dynamics and energy exchange processes would be very interesting.

Acknowledgment. We acknowledge C. Flytzanis for his very important help during this work and M. Achermann and S. Tzortzakis for their participation in the early stage of the experiments. We are also endebted to A. Nakamura, Y. Hamanaka, and S. Omi for helpful discussions and for providing some of the silver nanoparticle samples. We also thank B. Prével, M. Gaudry, E. Cottancin, J. Lermé, M. Pellarin, M. Broyer, M. Maillard, and M. P. Pileni for their help in the theoretical and experimental parts of this work and for providing us with very good quality samples.

References and Notes

(1) *Clusters*, *Science* **1997**, *271*, 967.

(2) *Nanostructured Materials: Clusters, Composites and Thin Films*; Shalaev, V. M., Moskovits, M., Eds.; American Chemical Society: Washington, DC, 1997.

(3) Henry, C. R. *Appl. Surf. Sci.* **2000**, *164*, 252.

(4) Haglund, R. F. In *Handbook of Optical Properties*; Hummel, R. E., Wissmann, P., Eds.; CRC Press: New York, 1997; Vol. 2, p 191.

(5) Kawabata, A.; Kubo, R. J. *Phys. Soc. Jpn.* **1966**, *21*, 1765.

(6) Genzel, L.; Martin, T. P.; Kreibig, U. *Z. Phys. B* **1975**, *21*, 339.

(7) Halperin, W. P. *Rev. Mod. Phys.* **1986**, *58*, 533.

(8) Flytzanis, C.; Hache, F.; Klein, M. C.; Ricard, D.; Roussignol, P. In *Progress in Optics*; Wold, E., Ed.; North-Holland: Amsterdam, 1991; Vol. XXIX, p 321.

(9) Kreibig, U.; Vollmer, M. *Optical Properties of Metal Clusters*; Springer: Berlin, 1995.

(10) Ricard, D. In *Nonlinear Optical Materials: Principles and Applications*; Degiorgio, V., Flytzanis, F., Eds.; IOS Press: Amsterdam, 1995; p 289.

(11) Vallée, F.; Del Fatti, N.; Flytzanis, C. In *Nanostructured Materials*; Shalaev, V. M.; Moskovits, M., Eds.; American Chemical Society: Washington, DC, 1997; p 70.

(12) Shalaev, V. M. *Phys. Rep.* **1996**, *272* 61.

(13) Elsayed-Ali, H. E.; Norris, T. B.; Pessot, M. A.; Mourou, G. A. *Phys. Rev. Lett.* **1987**, *58*, 1212.

(14) Schoenlein, R. W.; Lin, W. Z.; Fujimoto, J. G.; Eesley, G. L. *Phys. Rev. Lett.* **1987**, *58*, 1680.

(15) Sun, C. K.; Vallée, F.; Acioli, L. H.; Ippen, E. P.; Fujimoto, J. G. *Phys. Rev. B* **1994**, *50*, 15337 and references therein.

(16) Groeneveld, R.; Sprik, R.; Lagendijk, A. *Phys. Rev. B* **1995**, *51*, 11433.

(17) Brorson, S. D.; Kazeroonian, A.; Modera, J. S.; Face, D. W.; Cheng, T. K.; Ippen, E. P.; Dresselhaus, M. S.; Dresselhaus, G. *Phys. Rev. Lett.* **1990**, *64*, 2172.

(18) Elsayed-Ali, H. E.; Juhasz, T.; Smith, G. O.; Bron, W. E. *Phys. Rev. B* **1991**, *43*, 4488.

(19) Del Fatti, N.; Bouffanais, R.; Vallée, F.; Flytzanis, C. *Phys. Rev. Lett.* **1998**, *81*, 922.

(20) Del Fatti, N.; Voisin, C.; Achermann, M.; Tzortzakis, S.; Christofilos, D.; Vallée, F. *Phys. Rev. B* **2000**, *61*, 16956.

(21) Tokizaki, T.; Nakamura, A.; Kavelo, S.; Uchida, K.; Omi, S.; Tanji, H.; Asahara, Y. *Appl. Phys. Lett.* **1994**, *65*, 941.

(22) Bigot, J. Y.; Merle, J. C.; Cregut, O.; Daunois, A. *Phys. Rev. Lett.* **1995**, *75*, 4702.

(23) Zhang, J. Z. *Acc. Chem. Res.* **1997**, *30*, 423 and references therein.

(24) Nisoli, M.; Stagira, S.; De Silvestri, S.; Stella, A.; Tognini, P.; Cheyssac, P.; Kofman, R. Phys. *Rev. Lett.* **1997**, *78*, 3575.

(25) Perner, M.; Bost, P.; Lemmer, U.; von Plessen, G.; Feldmann, J.; Becker, U.; Mennig, M.; Schmitt, M.; Schmidt, H. *Phys. Rev. Lett.* **1997**, *78*, 2192.

(26) Inouye, H.; Tanaka, K.; Tanahashi, I.; Hirao, K. *Phys. Rev. B* **1998**, *57*, 11334.

(27) Hamanaka, Y.; Nakamura, A.; Omi, S.; Del Fatti, N.; Vallée, F.; Flytzanis, C. *Appl. Phys. Lett.* **1999**, *75*, 1712.

(28) Del Fatti, N.; Vallée, F.; Flytzanis, C.; Hamanaka, Y.; Nakamura, A. *Chem. Phys.* **2000**, *251*, 215.

(29) Hodak, J. H.; Martini, I.; Hartland, G. V. *J. Phys. Chem. B* **1998**, *102*, 6958.

(30) Hodak, J. H.; Henglein, A.; Hartland, G. V. *J. Chem. Phys.* **1999**, *111*, 8613.

(31) Link, S.; El-Sayed, M. A. *J. Phys. Chem. B* **1999**, *103*, 8410.

(32) Voisin, C.; Christofilos, D.; Del Fatti, N.; Vallée, F.; Prével, B.; Cottancin, E.; Lermé, J.; Pellarin, M.; Broyer, M. *Phys. Rev. Lett.* **2000**, *85*, 2200.

(33) Beaurepaire, E.; Merle, J. C.; Daunois, A.; Bigot, J. Y. *Phys. Rev. Lett.* **1996**, *76*, 4250.

(34) Hohlfeld, J.; Matthias, E.; Knorren, R.; Bennemann, K. H. *Phys. Rev. Lett.* **1997**, *78*, 4861.

(35) Ju, G.; Vertikov, A.; Nurmikko, A. V.; Canady, C.; Xia, G.; Farrow, R. F. C.; Cebollada, A. *Phys. Rev. B* **1998**, *57*, R700.

(36) Beaurepaire, E.; Maret, M.; Halté, V.; Merle, J. C.; Daunois, A.; Bigot, J. Y. *Phys. Rev. B* **1998**, *58*, 12134.

(37) Brorson, S. D.; Fujimoto, J. G.; Ippen, E. P. *Phys. Rev. Lett.* **1987**, *59*, 1962.

(38) Suarez, C.; Bron, W. E.; Juhasz, T. *Phys. Rev. Lett.* **1995**, *75*, 4536.

(39) Nisoli, M.; De Silvestri, S.; Cavalleri, A.; Malvezzi, A. M.; Stella, A.; Lanzani, G.; Cheyssac, P.; Kofman, R. *Phys. Rev. B* **1997**, *55*, R13424.

(40) Hodak, J. H.; Martini, I.; Hartland, G. V. *J. Chem. Phys.* **1998**, *108*, 9210.

(41) Del Fatti, N.; Voisin, C.; Chevy, F.; Vallée, F.; Flytzanis, C. *J. Chem. Phys.* **1999**, *110*, 11484.

(42) Voisin, C.; Del Fatti, N.; Christofilos, D.; Vallée, F. *Appl. Surf. Sci.* **2000**, *164*, 131.

(43) Del Fatti, N.; Voisin, C.; Christofilos, D.; Vallée, F.; Flytzanis, C. *J. Phys. Chem. A* **2000**, *104*, 4321.

(44) Heilweil, E. J.; Hochstrasser, R. M. *J. Chem. Phys.* **1985**, *82*, 4762.

(45) Bloemer, M. J.; Haus, J. W.; Ashley, P. R. *J. Opt. Soc. Am. B* **1990**, *7*, 790.
(46) Haglund, R. F.; Lupke, G.; Osborne, D. H.; Chen, H.; Magruder, R. H.; Zuhr, R. A. In *Ultrafast Phenomena XI*; Elsaesser, T., Fujimoto, J. G., Wiersma, D. A., Zinth, W., Eds.; Springer-Verlag: Berlin, 1998; p 356.
(47) Ashcroft, N. W.; Mermin, N. D. *Solid State Physics*; Saunders College: Philadelphia, 1976.
(48) Johnson, P. B.; Christy, R. W. *Phys. Rev. B* **1972**, *6*, 4370.
(49) Smith, J. B.; Ehrenreich, H. *Phys. Rev. B* **1982**, *25*, 923.
(50) Gurzhi, R. N. *Sov. Phys. JETP* **1959**, *35*, 673.
(51) Tsai, C.-Yi; Tsai, C.-Yao; Chen, C.-H.; Sung, T.-L.; Wu, T.-Y.; Shih, F.-P. *IEEE J. Quantum Electron.* **1998**, *34*, 552.
(52) Kaveh, M.; Wiser, N. *Adv. Phys.* **1984**, *33*, 257.
(53) Ehrenreich, H.; Philipp, H. R. *Phys. Rev.* **1962**, *128*, 1622.
(54) Perenboom, J. A. A.; Wyder, P.; Meier, F. *Phys. Rep.* **1981**, *78*, 173.
(55) Hache, F.; Ricard, D.; Flytzanis, C. *J. Opt. Soc. Am. B* **1986**, *3*, 1647.
(56) Kreibig, U. In *Handbook of Optical Properties*; Hummel, R. E.; Wissmann, P., Eds.; CRC Press: New York, 1997; Vol. 2, p 145.
(57) Hovel, H.; Fritz, S.; Hilger, A.; Kreibig, U.; Vollmer, M. *Phys. Rev. B* **1993**, *48*, 18178.
(58) Doremus, R. H. *J. Chem. Phys.* **1965**, *42* 414.
(59) Maxwell−Garnett, J. C. *Philos. Trans. R. Soc. London* **1904**, *203*, 385; **1906**, *205*, 237.
(60) Mie G. *Ann. Phys.* **1908**, *25*, 377.
(61) Born, M.; Wolf, E. *Principles of Optics*; Pergamon: Oxford, U.K., 1975.
(62) Mills, D. L.; Burstein, E. *Rep. Prog. Phys.* **1974**, *37*, 817.
(63) Hollstein, T.; Kreibig, U.; Leis, F. *Phys. Stat. Sol. b* **1977**, *82*, 545.
(64) Jain, S. C.; Arora, N. D. *J. Phys. Chem. Solids* **1974**, *35*, 1231.
(65) Genzel, L.; Martin, T. P.; Kreibig, U. *Z. Phys. B* **1975**, *21*, 339.
(66) Lermé, J.; Palpant, B.; Prével, B.; Pellarin, M.; Treilleux, M.; Vialle, J. L.; Perez, A.; Broyer, M. *Phys. Rev. Lett.* **1998**, *80*, 5105.
(67) Lermé, J.; Palpant, B.; Prével, B.; Cottancin, E.; Pellarin, M.; Treilleux, M.; Vialle, J. L.; Perez, A.; Broyer, M. *Eur. Phys. J. D* **1998**, *4*, 95.
(68) Lamprecht, B.; Leitner, A.; Aussenegg, F. R. *Appl. Phys. B* **1999**, *68*, 419.
(69) Lamprecht, B.; Krenn, J. R.; Leitner, A.; Aussenegg, F. R. *Phys. Rev. Lett.* **1999**, *83*, 4421.
(70) Vartanyan, T.; Simon, M.; Träger, F. *Appl. Phys. B* **1999**, *68*, 425.
(71) Stietz, F.; Bosbach, J.; Wenzel, T.; Vartanyan, T.; Goldmann, A.; Träger, F. *Phys. Rev. Lett.* **2000**, *84*, 5644.
(72) Voisin, C.; Christofilos, C.; Del Fatti, N.; Vallée, F *Eur. Phys. J. D*, to be published.
(73) Fann, W. S.; Storz, R.; Tom, H. W. K.; Bokor, J. *Phys. Rev. Lett.* **1992**, *68*, 2834; *Phys. Rev. B* **1992**, *46*, 13592.
(74) Aeschlimann, M.; Bauer, M.; Pawlik, S. *Chem. Phys.* **1996**, *205*, 127.
(75) Aeschlimann, M.; Bauer, M.; Pawlik, S.; Weber, W.; Burgermeister, R.; Oberli, D.; Siegmann, H. C. *Phys. Rev. Lett.* **1997**, *79*, 5158.
(76) Ogawa, S.; Nagano, H.; Petek, H. *Phys. Rev. B* **1997**, *55*, 10869.
(77) Knoesel, A.; Hotzel, A.; Wolf, M. *Phys. Rev. B* **1998**, *57*, 12812.
(78) Cao, J.; Cao, Y.; Elsayed-Ali, H. E.; Miller, R. J. D.; Mantell, D. A. *Phys. Rev. B* **1998** *58*, 10948.
(79) Sun, C. K.; Vallée, F.; Acioli, L. H.; Ippen, E. P.; Fujimoto, J. G. *Phys. Rev. B* **1993**, *48*, 12365.
(80) Logunov, S. L.; Ahmadi, T. S.; El-Sayed, M. A.; Khoury, J. T.; Whetten, R. L. *J. Phys. Chem. B* **1997**, *101*, 3713.
(81) Link, S.; Burda, C.; Wang, Z. L.; El-Sayed, M. A. *J. Chem. Phys.* **1999**, *111*, 1255.
(82) Hodak, J. H.; Henglein, A.; Hartland, G. V. *J. Chem. Phys.* **2000**, *112*, 5942.
(83) Kaganov, M. I.; Lifshitz, I. M.; Tanatarov, L. V. *Zh. Eksp. Teor. Fiz.* **1957**, *31*, 232 [*Sov. Phys. JETP* **1957**, *4*, 173].
(84) Del Fatti, N.; Flytzanis, C.; Vallée, F. *Appl. Phys. B* **1999**, *68*, 433.
(85) Petek, H.; Nagano, H.; Ogawa, S. *Phys. Rev. Lett.* **1999**, *83*, 832.
(86) Rosei, R. *Phys. Rev. B* **1974**, *10*, 474.
(87) Rosei, R.; Culp, C. H.; Weaver, J. H. *Phys. Rev. B* **1974**, *10*, 484.
(88) Rosei, R.; Antonangeli, F.; Grassano, U. M. *Surf. Sci.* **1973**, *37*, 689.
(89) Christensen, N. E.; Seraphin, B. O. *Phys. Rev. B* **1971**, *4*, 3321.
(90) Rosei, R.; Lynch, D. W. *Phys. Rev. B* **1972**, *5*, 3883.
(91) Uchida, K.; Kaneko, S.; Omi, S.; Hata, C.; Tanji, H.; Asahara, Y.; Ikushima, A. J.; Tokisaki, T.; Nakamura, A. *J. Opt. Soc. Am. B* **1994**, *11*, 1236.
(92) Palpant, B.; Prével, B.; Lermé, J.; Cottancin, E.; Pellarin, M.; Treilleux, M.; Perez, A.; Vialle, J. L.; Broyer, M. *Phys. Rev. B* **1998**, *57*, 1963.
(93) Rosei, R.; Lynch, D. W. *Phys. Rev. B* **1972**, *5*, 3883.
(94) Halté, V.; Guille, J.; Merle, J. C.; Perakis, I.; Bigot, J. Y. *Phys. Rev. B* **1999**, *60*, 11738.
(95) Hartland, G. V.; Hodak, J. H.; Martini, I. *Phys. Rev. Lett.* **1999**, *82*, 3188.
(96) Perner, M.; Von Plessen, G.; Feldmann, J. *Phys. Rev. Lett.* **1999**, *82*, 3188.
(97) Shahbazyan, T. V.; Perakis, I. E.; Bigot, J. Y. *Phys. Rev. Lett.* **1998**, *81*, 3120.
(98) Shahbazyan, T. V.; Perakis, I. E. *Phys. Rev. B* **1999**, *60*, 9090.
(99) Collet, J. H. *Phys. Rev. B* **1993**, *47*, 10279.
(100) Ekardt, W. *Phys. Rev. B* **1984**, *29*, 1558.
(101) Bréchignac, C.; Cahuzac, P.; Leygnier, J.; Sarfati, A. *Phys. Rev. Lett.* **1993**, *70*, 2036.
(102) Liebsch, A. *Phys. Rev. B* **1993**, *48*, 11317.
(103) Pines, D.; Nozières, P. *The Theory of Quantum Liquids*; Benjamin: New York, 1966.
(104) Bürgi, L.; Jeandupeux, O.; Brune, H.; Kern, K. *Phys. Rev. Lett.* **1999**, *82*, 4516.
(105) Roberti, T. W.; Smith, B. A.; Zhang, J. Z. *J. Chem. Phys.* **1995**, *102*, 3860.
(106) Halté, V.; Bigot, J. Y.; Palpant, B.; Broyer, M.; Prével, B.; Pérez, A. *Appl. Phys. Lett.* **1999**, *75*, 3799.
(107) Smith, B. A.; Zhang, J. Z.; Giebel, U.; Schmid, G. *Chem. Phys. Lett.* **1997**, *270*, 139.
(108) Link, S.; Burda, C.; Mohamed, M. B.; Nikoobakht, B.; El-Sayed, M. A. *Phys. Rev. B* **2000**, *61*, 6086.
(109) Averitt, R. D.; Westcott, S. L.; Hallas, N. J. *Phys. Rev. B* **1998**, *58*, R10203.
(110) Stella, A.; Nisoli, M.; De Silvestri, S.; Svelto, O.; Lanzani, G.; Cheyssac, P.; Kofman, R. *Phys. Rev. B* **1996**, *53*, 15497.
(111) Klein-Wiele, J. H.; Simon, P.; Rubahn, H. G. *Phys. Rev. Lett.* **1998**, *80*, 45.
(112) Liu, D.; He, P.; Alexander, D. R. *Appl. Phys. Lett.* **1993**, *62*, 249.
(113) Belotskii, E. D.; Tomchuk, P. M. *Surf. Sci.* **1990**, *239*, 143.
(114) Belotskii, E. D.; Tomchuk, P. M. *Int. J. Electron.* **1992**, *73*, 955.
(115) Takagahara, T. *J. Lumin.* **1996**, *70*, 129.
(116) Lamb, H. *Proc. London Math. Soc.* **1882**, *13*, 189.
(117) Tamura, A.; Higeta, K.; Ichinokawa, T. *J. Phys. C* **1982**, *15*, 4975.
(118) Tamura, A.; Ichinokawa, T. *J. Phys. C* **1983**, *16*, 4779.
(119) Nishiguchi, N.; Sakuma, T. *Sol. State Comm.* **1981**, *38*, 1073.
(120) Dubrovskiy, V. A.; Morochnik, V. S. *Earth Phys.* **1981**, *17*, 494.
(121) Satô, Y.; Usami, T. *Geophys. Magn.* **1962**, *31*, 15.
(122) Baltes, H. P.; Hilf, E. R. *Solid State Comm.* **1973**, *12*, 369.
(123) Kara A.; Rahman, T. S. *Phys. Rev. Lett.* **1998**, *81*, 1453.
(124) Fu, H.; Ozolins, V.; Zunger, A. *Phys. Rev. B* **1999**, *59*, 2881.
(125) Saviot, L.; Champagnon, B.; Duval, E.; Ekimov, A. I. *Phys. Rev. B* **1998**, *57*, 341; and references therein.
(126) Fujii, M.; Nagareda, T.; Hayashi, S.; Yamamoto, K. *Phys. Rev. B* **1991**, *44*, 6243.
(127) Felidj, N.; Aubard, J.; Lévi, G. *J. Chem. Phys.* **1996**, *104*, 9735.
(128) Palpant, B.; Portales, H.; Saviot, L.; Lermé, J.; Prével, B.; Pellarin, M.; Duval, E.; Perez, A.; Broyer, M. *Phys. Rev. B* **1999**, *60*, 17107.
(129) Krauss, T. D.; Wise, F. W. *Phys. Rev. Lett.* **1997**, *79*, 5102.
(130) Thoen, E. R.; Steinmeyer, G.; Langlois, P.; Ippen, E. P.; Tudury, G. E.; Brito Cruz, C. H.; Barbosa, L. C.; Cesar, C. L. *Appl. Phys. Lett.* **1998**, *73*, 2149.
(131) Perrin, B.; Rossignol, C.; Bonello, B.; Jeannet, J. C. *Physica B* **1999**, *263*−*264*, 571.
(132) Perner, M.; Gresillon, S.; März, J.; Von Plessen, G.; Feldmann, J.; Porstendorfer, J.; Berg, K. J.; Berg, G. *Phys. Rev. Lett.* **2000**, *85*, 792.
(133) Hodak, J. H.; Henglein, A.; Hartland, G. V. *J. Phys. Chem. B* **2000**, *104*, 5053.
(134) Yan, Y. X.; Gamble, E. B.; Nelson, K. A. *J. Chem. Phys.* **1985**, *83*, 5391.
(135) Merlin, R. *Solid State Commun.* **1997**, *102*, 207.
(136) Zeiger, H. J.; Vidal, J.; Cheng, T. K.; Ippen, E. P.; Dresselhaus, G.; Dresselhaus, M. S. *Phys. Rev. B* **1992**, *45*, 768.
(137) Kutt, W. A.; Albrecht, W.; Kurz, H *IEEE J. Quantum Elec.* **1992**, *28*, 2434.
(138) Thomsen, C.; Grahn, H. T.; Maris, H. J.; Tauc, T. J. *Phys. Rev. B* **1986**, *34*, 4129.
(139) Wright, O. B. *Phys. Rev. B* **1994**, *49*, 9985.
(140) Gusev, V. E. *Opt. Comm.* **1992**, *94*, 76.
(141) Yamamoto, A.; Mishina, T.; Masumoto, Y. *Phys. Rev. Lett.* **1994**, *73*, 740.
(142) Bartels, A.; Dekorsy, T.; Kurz, H.; Köhler, K *Phys. Rev. Lett.* **1999**, *82*, 1044.
(143) Banin, U.; Cerullo, G.; Guzelian, A. A.; Bardeen, C. J.; Alivisatos, A. P.;, Shank, C. V. *Phys. Rev. B* **1997**, *55*, 7059.
(144) Sun, C. K.; Liang, J. C.; Yu, X. Y. *Phys. Rev. Lett.* **2000**, *84*, 179.
(145) Barron, T. H. K.; Collins, J. G.; White, G. K. *Adv. Phys.* **1980**, *29*, 609.
(146) Fierz, M.; Siegmann, K.; Scharte, M.; Aeschlimann, M. *Appl. Phys. B* **1999**, *68*, 415.

(147) Klar, T.; Perner, M.; Grosse, S.; Von Plessen, G.; Spirkl, W.; Feldmann, J. *Phys. Rev. Lett.* **1998**, *80*, 4249.
(148) Nechay, B. A.; Siegner, U.; Morier-Genoud, F.; Schertel, A.; Keller, U. *Appl. Phys. Lett.* **1999**, *74*, 61.
(149) Guenther, T.; Emiliani, V.; Intonti, F.; Lienau, C.; Elsaesser, T.; Nötzel, R.; Ploog, K. H. *Appl. Phys. Lett.* **1999**, *75*, 3500.
(150) Taleb, A.; Petit, C.; Pileni, M. P. *Chem. Mater.* **1997**, *9*, 950.
(151) Krenn, J. R.; Dereux, A.; Weeber, J. C.; Bourillot, E.; Lacroute, Y.; Goudonnet, J. P.; Schider, G.; Gotschy, W.; Leitner, A.; Aussenegg, F. R.; Girard, C. *Phys. Rev. Lett.* **1999**, *82*, 2590.
(152) Lamprecht, B.; Schider, G.; Lechner, R. T.; Ditlbacher, H.; Krenn, J. R.; Leitner, A.; Aussenegg, F. R. *Phys. Rev. Lett.* **2000**, *84*, 4721.
(153) Silly, F.; Gusev, A. O.; Taleb, A.; Charra, F.; Pileni, M. P. *Phys. Rev. Lett.* **2000**, *84*, 5840.